Electrorheological Brake for Haptic Interface Systems

A Thesis
Presented to
The Academic Faculty

by

Priya Vallabh

In Partial Fulfillment
of the Requirements for the Degree

Master of Science

in the School of Mechanical Engineering

Georgia Institute of Technology
August 2002

Electrorheological Brake for Haptic Interface Systems

Approved:

_____

Dr. Wayne J. Book , Committee Chair

_____

Dr. Aldo Ferri

_____

Dr. Scott Bair

Date Approved _____

To Rohit ...

ACKNOWLEDGEMENTS

I thank Dr. Wayne Book for his support and assistance throughout the duration of this project. His guidance and experience were invaluable.

Acknowledgement also has to made to the personnel in the Machine and Electrical shops. Their assistance with the construction of the test apparatus was appreciated.

My thanks also go out to my fellow IMDL colleagues as well as all my friends at the Georgia Institute of Technology, for their friendship, insight, support and motivation.

Last but not least, I would like to thank my husband, for motivating me to take this step, towards attaining my masters degree.

TABLE OF CONTENTS

LIST OF TABLES

LIST OF FIGURES

SUMMARY

This research investigates the feasibility of using electrorheological (ER) brakes in passive haptic systems. An ER brake was designed and built. Various tests performed revealed that the brake did not respond as predicted, displaying slower response times than those being reported in literature. The poor performance was attributed to slow strain rates used during the testing process.

An increase in torque was also noted at low strain rates. This phenomenon was thoroughly investigated and a conclusion was reached that open loop control will not be possible for haptic application.

Simple proportional feed back control was implemented and this resulted in a considerable decrease in rise time of the brake.

With increased speed and implementation of feedback control, rise times similar to those reported in literature for high speed clutches will be attainable.

A conceptual design for a three degree of freedom ER haptic test bed is also presented.

CHAPTER I

INTRODUCTION

1.1 Research Basis

A haptic interface device, (joy stick, mouse or robotic manipulator) feeds back the sensation of force to the user, while performing a task. The task could be tele-operation or simulation of a virtual environment.

Haptic interfaces are categorized as either active or passive depending on the nature of the force feedback mechanism used. Active devices use motors to actively restrict motion. This could be harmful if the energy produced by this device is large enough to overpower the user. Passive devices on the other hand use actuators that dissipate, store or redirect user supplied energy [15]. Passive devices are from this respect more desirable.

PTER (Passive Trajectory Enhancing Robot) is a passive haptic test bed developed at Georgia Tech. PTER utilizes modified magnetic friction clutches to provide the torque required for force feedback. Tests performed on PTER revealed that stiction in the clutches (caused by the transition between static and dynamic friction) resulted in discontinuous braking torques [15].

Various other braking devices such as hysteresis clutches, eddy current clutches and hydraulically and pneumatically actuated units were investigated by Tognetti [23] and found to be unsuitable. Hysteresis clutches were rejected because of their cogging phenomena and current vs. torque hysteresis characteristics, eddy current clutches were rejected because of their torque slip characteristics which prevented them from applying torque at low speeds, hydraulic units were rejected because of their impact on the environment while pneumatic units were rejected because it was hypothesized that compressible fluids would hinder band width capabilities, preventing quick modulation of applied torque.

A new type of passive braking device is needed for haptic interface systems. It is believed that devices based on electrorheological fluids will be able to fill this gap.

Electrorheological (ER) fluids are fluids which experience a rapid, reversible change in apparent viscosity when subjected to large electrical fields. Utilizing this property together with their quick response times, a fast acting brake with minimal residual friction can be designed.

The objective of the current research was to therefore, experimentally investigate the properties of ER fluids, in order to determine their feasibility, as the working medium in haptic interface braking systems.

1.2 Introduction to Electrorheological fluids

The ER effect was first reported in 1947 by Willis Winslow. Winslow discovered that applying a large electrical field to a solution of non aqueous silica suspensions, which was activated by small quantities of water, resulted in an increase in viscosity of the fluid [10]. He demonstrated that such fluids exhibited fast response times and were capable of being used as the working medium in devices such as brakes, dampers, clutches and hydraulic equipment [6].

ER fluids can be classified into two basic types:

- Particle Type
- Homogeneous Type

Particle type ER fluids are typically suspensions of particles in a viscous, non conducting base oil with a particle-fluid dielectric mismatch [2]. With no electric field, the particles are evenly distributed within the fluid. The fluid exhibits Newtonian characteristics i.e. stress is directly proportional to strain rate. This is shown in figure 1 a. This proportionality constant is called the zero field viscosity or plastic viscosity, η_{pl}.

When an electric field is applied, a change in 'apparent viscosity' is noticeable, however the plastic viscosity remains approximately constant across all field ranges [6], while the resulting shear stress needed for flow to commence, increases. (The term 'apparent viscosity' is used to describe a rheological parameter of ER fluids. A definition of this term will be given in section 2.1.1).

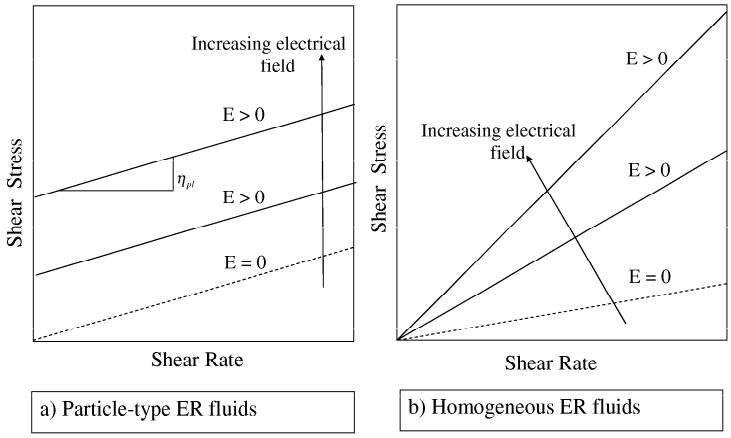

Figure 1: Stress vs. Strain Rate relationship of particle and homogeneous ER fluids.

With the application of an electrical field, the particles in the fluid polarize and form chains, called fibrils, in the direction of the electric field. Relative motion of the fluid causes these fibrils to break and re-form, resulting in a force that resists motion [22]. This force is responsible for resulting in a field dependant component of shear. Figure 2 show the effect that an electric field has on the particles within ER fluids.

The size and shape of these particle vary between different types of ER fluids. Different sizes and shapes of particles result in different ER fluid properties. Typical particle sizes range from 0.04 to 50 μm.

Homonegous type ER fluids discussed by Furusho and Sakaguchi [17], are developed using low molecular weight liquid crystal or macromolecular liquid crystal. Here shear stress is directly proportional to shear strain rate, with the constant of proportionality increasing with increasing electrical field. (Essentially, the plastic viscosity is controlled by the electrical field.) Figure 1 b) shows a typical stress vs. strain rate curve for these types of ER fluids.

Particle type ER fluids were tested in this research, so future reference to 'ER fluids' would indicate 'particle type ER fluid'.

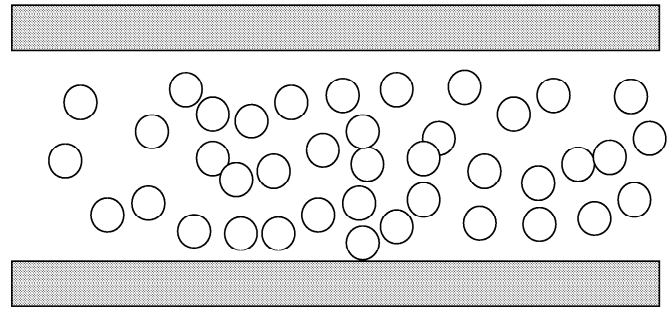

a) No electric field

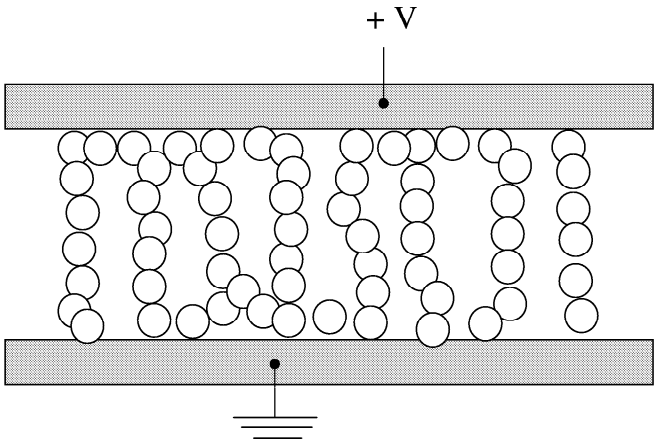

b) With electric field

Figure 2: Effect of electrical field on particle type ER fluids.

CHAPTER II

LITERATURE SURVEY

Extensive research has been done on electrorheological fluids, their properties and their development. This literature search focuses on previous work done in the following areas:

- ER fluid theory
- The use of ER fluids in clutches
- ER fluids in haptic interface systems
- The modeling of ER fluids

2.1 ER Fluid Theory

2.1.1 Rheological Parameters of ER fluids

ER fluids behave like Coulomb friction i.e. initiating motion requires that some static yield stress has to first be overcome, before motion occurs. Once motion occurs, the static yield stress falls quickly to the dynamic value. Figure 3 shows the behavior of static and dynamic yield stress plotted against strain rate. Friction is also shown here to portray the similarities between yield stress and friction. Friction is independent of velocity; this is seen in the flat curve in Figure 3, while shear stress is dependent on velocity with the slope of the curve being the plastic viscosity.

Three steps in the process to yielding occur: pre-yield, yield and post-yield. In the pre-yield region, application of stress results in little or no motion. The fluid behaves as a visco-elastic solid in this region. As the stress is increased, the material deforms beyond the yield point, and enters the plastic region where flow commences. An idealized depiction of the pre-yield and post-yield characteristics of ER fluids is shown in Figure 4.

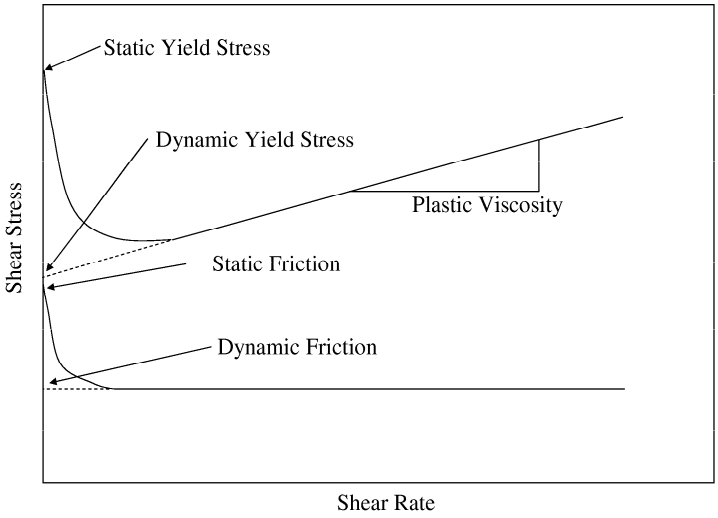

Figure 3: Idealized representation of static and dynamic yield stress.

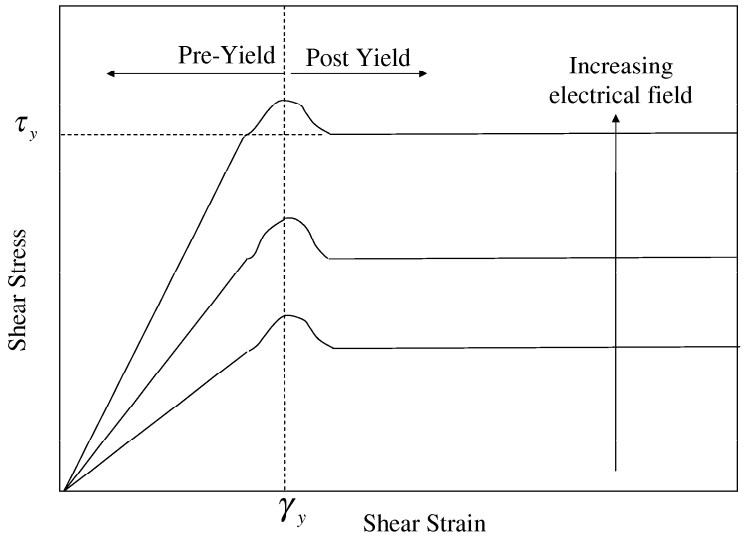

Figure 4: Idealized stress vs. strain curves [8].

Three basic rheological parameters describe the ER transition [10]:

- Yield Stress
- Steady Shear Viscosity
- Dynamic Modulus

The post *yield stress* behavior of ER fluids is often modeled using the Bingham plastic approximation in Equation 1 [8].

$$\tau = sgn(\dot{\gamma})\tau_y + \eta_{pl}\dot{\gamma} \tag{1}$$

Here, τ_y is dynamic yield stress, $\dot{\gamma}$ is strain rate and η_{pl} is plastic viscosity. The dynamic yield strength is a function of electric field, while the plastic viscosity remains more or less constant over the entire electrical field range [10]. (Note that this is not always the case since the plastic yield stress is shown to vary with electrical field for certain fluids.) Dynamic yield stress increases with increasing field strength and according to Srinivasan and Mcfarland [22], it is typically proportional to the field strength raised to a power between 1 & 2. The relationship that is most widely used in literature is:

$$\tau_y(E) = \alpha E^2 \tag{2}$$

where α is a fluid constant that needs to be determined experimentally.

The *steady shear viscosity* (or apparent viscosity) is described as:

$$\eta_A = \frac{\tau}{\dot{\gamma}} \tag{3}$$

In Newtonian fluids this viscosity is constant, however non-Newtonian fluids, display a shear rate dependent viscosity which can be either pseudo plastic (shear-thinning) or dilatant (shear-thickening). According to Jordan and Shaw [10], ER fluids tend to be pseudo plastic i.e. their apparent viscosity decreases as shear rate increases. Figure 5 shows the stress strain behavior for various types od fluids. ER fluids display a combination of pseudo plastic and Bingham plastic characteristics.

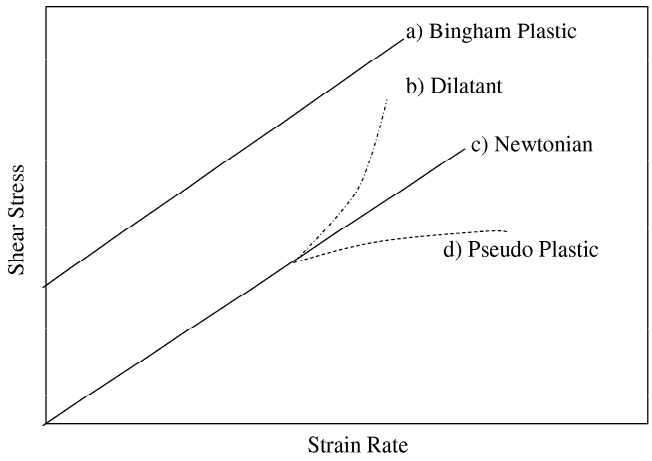

Figure 5: Shear stress vs. strain rate behaviour for various fluid types.

Another interesting fact Jordan and Shaw [10] mention, is that at low shear rates, η_A is directly proportional to $\frac{\tau}{\dot{\gamma}}$, therefore in strong fields and at low shear rates, ER fluids display a solid like nature, since shear stress remains constant.

Visco-elastic materials, produce stress components that are both in phase and out of phase to the applied strain, when subjected to sinusoidal deformations [10]. (An elastic material would produce components that are in phase, while a viscous material would produce components that are 90° out of phase to the strain input.)

Visco-elastic materials are therefore described by the *complex dynamic modulus*:

$$G^* = G' + iG'' \tag{4}$$

G' is referred to as the storage (in phase) modulus and G'' is the loss modulus (out of phase).

2.1.2 ER Device Electrode Configuration

Two types of electrode configurations are available for ER devices:

- Fixed Electrode Configuration

- Sliding Electrode Configuration

In the fixed electrode configuration, shown in Figure 6, the electrodes are stationary and set a fixed distance apart. The fluid flows between the electrodes at a flow rate induced

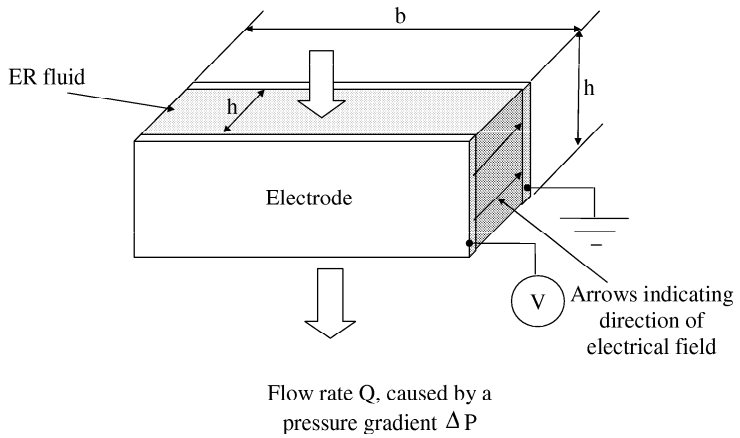

Figure 6: A schematic of the fixed electrode configuration.

by a pressure gradient. The voltage across the electrode gap is controlled, which in turn controls the shear rate of the fluid and hence the pressure drop. A typical use of this type of electrode arrangement would be an ER valve in a hydraulic circuit in which the working fluid is ER fluid.

In the sliding electrode configuration, shown in Figure 7, parallel electrodes with ER fluid between them move relative to each other at a specific speed (S) when subjected to a shear force (F). Devices utilizing this type of arrangement include brakes and clutches. Coulter, Weiss and Carlson[8], give a good description of the theoretical analysis which is briefly discussed below:

Force, F, and shear stress, τ, are related in the following way:

$$F = \tau A \tag{5}$$

where A, is the electrode surface area. The shear stress, τ is determined from Equation 1.

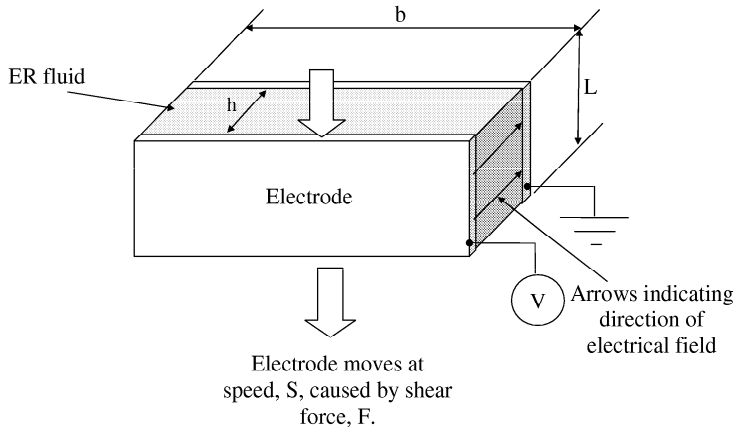

Figure 7: A schematic of the sliding electrode configuration.

Assuming a linear velocity distribution with the velocity differential across the electrodes being, S, the shear rate can be described as:

$$\dot{\gamma} = \frac{S}{h} \tag{6}$$

where h, is the distance between the electrodes. Note that by combining Equations 1, 5 and 6, together with the electrode surface area, $A = Lb$, the force-speed relationship is obtained as shown in Equation 7.

$$F = Lb\tau_y sgn(S) + \frac{SLb\eta}{h} \tag{7}$$

The first term in Equation 7 describes the contribution to the transmitted force caused by the yield stress of the ER fluid, while the second term is called the viscous force term. This is the force that is due to the velocity of the electrode.

It should be noted that the above theory is only valid if the parallel planar configuration is utilized. Section 2.1.4 discusses the changes that need to be made to Equation 7 for a concentric cylinder geometry.

2.1.3 ER Clutch/Brake Geometries

All ER clutch and brake geometries are based on the parallel electrode configuration. These are best discussed pictorially and are shown in Figure 8.

The types a), b) and f) are mainly used for test purposes to determine the properties of ER fluids. These basically have one input rotating member transmitting toque through the ER fluid to the output member. In Figure 8, the ER fluid occupies the regions which have been shaded in.

Type c) and d) are extensions of the aforementioned types, which maximize on surface area, resulting in larger shearing surface areas and hence torque. It should be noted though that a larger surface area would require a larger current density and hence a larger power supply, therefore when designing, a good balance needs to be maintained between surface area and torque. One advantage of using these types of arrangements is that smaller devices can be designed.

Type e) is of the type presented by Böse and Berkemeier [3]. The solid spherical shape resulted in the inertia of the system being too large, thus affecting the performance of the clutch. This is discussed in Section 2.2.1.

2.1.4 Theory of Flow in Concentric Clutches

Atkin, Shi and Bullough [1] discuss how the theory presented in section 2.1.2 can be adapted for the concentric cylinder type electrode arrangement. Since the clutch used in the current research was of this type, this theory is presented in detail below.

In Figure 9, flow is caused by the outer cylinder which is rotating at an instantaneous angular speed, Ω, produced by a torque, T. The inner cylinder is fixed. Let $\omega(r)$ be the angular speed of a point in the fluid at a distance, r, from the axis of the cylinders, then $v_r = 0$, $v_\theta = r\omega(r)$ and $v_z = 0$.

The shear stress as given by Equation 1 is written here as:

$$\tau_{r\theta} = \tau_y sgn\left(\frac{d\omega}{dr}\right) + \eta_{pl} r \frac{d\omega}{dr} \tag{8}$$

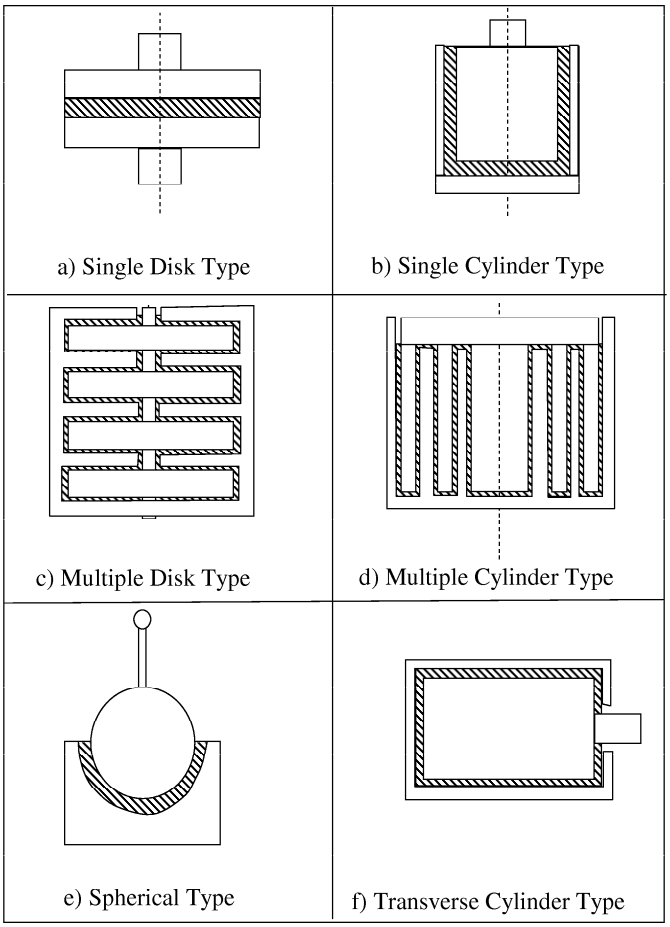

Figure 8: Various electrode geometries that have been used for ER clutches and brakes.

Torque, T, is related to shear stress in the following way:

$$\tau_{r\theta} = \frac{T}{2\pi L r^2} \tag{9}$$

where L, is the length of the cylinder. It follows that $\tau_{r\theta}$ is a decreasing function of r and,

$$\frac{T}{2\pi L R_2^2} < \tau_{r\theta} < \frac{T}{2\pi L R_1^2} \tag{10}$$

where R_1 is the radius of the inner cylinder and R_2 is the radius of the outer cylinder. Note that flow occurs if $\tau_{r\theta} > \tau_y$.

For concentric cylinders it is shown in [1] that the electric field, E, can be written as:

$$E = \frac{V}{ln(\frac{R_2}{R_1})}\frac{1}{r} \tag{11}$$

where the ratio $\frac{R_2}{R_1}$ is known as the geometry ratio.

The relationship between the magnitude of the electric field, E, and the yield stress, τ_y is given as:

$$\tau_y = \alpha E^2 \text{ or } \tau_y = \begin{cases} \alpha^*(E - E_0); & E > E_0 \\ 0; & E < E_0 \end{cases} \tag{12}$$

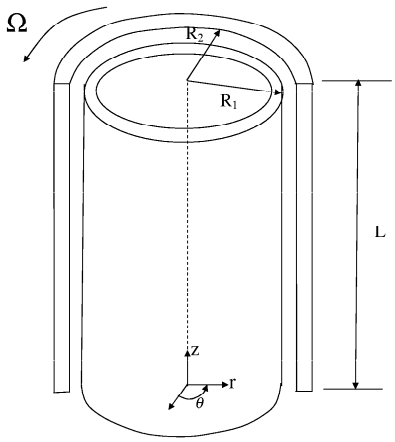

Figure 9: A schematic of the cylindrical clutch arrangement.

where α, α^* and E_0 are ER fluid constants. The following equation for yield stress is obtained by combining Equations 11 and 12:

$$\tau_y = \frac{C}{r^2} \; where \; C = \alpha \left(\frac{V}{ln(\frac{R_2}{R_1})} \right)^2 \tag{13}$$

Now at any radius, $\tau_{r\theta} > \tau_y$ only when $T > T_y$, where $T_y = 2\pi LC$, is the torque at the yield stress.

When $T > T_y$, there is flow across the entire gap and angular speed is given by

$$\omega = \frac{\Omega R_1^2 R_2^2}{R_1^2 - R_2^2} \left(\frac{1}{R_1^2} - \frac{1}{r^2} \right) \tag{14}$$

Equation 14 is the classical Newtonian velocity profile. The relationship between applied torque and angular speed can be now be written as:

$$T = T_y sgn(\Omega) + \frac{4\pi\eta\Omega L R_1^2 R_2^2}{R_1^2 - R_2^2} \tag{15}$$

Note that the form of the above equation is the same as that in Equation 7. The form of C in Equation 13 does not change if the grounded cylinder is the inner or outer. The solution for ω however changes depending on whether the inner or outer cylinder rotates which is the same as in the Newtonian case. When the inner cylinder rotates with speed Ω and the outer one is fixed then Equation 16, holds.

$$\omega = \frac{\Omega R_1^2 R_2^2}{R_2^2 - R_1^2} \left(\frac{1}{r^2} - \frac{1}{R_2^2} \right) \tag{16}$$

2.2 ER fluids in Haptic Interface Systems

2.2.1 Joy Stick Haptic device : Passive Device

Böse and Berkemeir [3] discuss a two degree of freedom haptic device that was developed and tested by them. The entire system consists of a spherical shaped ER actuator (resembling a joystick), a microcontroller and a computer.

The actuator consists of a spherical electrode mounted within a concentric half-spherical electrode. The two electrodes are separated by spacers allowing a gap width of 1 mm. A handle connected to the inner sphere allows direct maneuverability of the device.

The haptic joystick was capable of producing a maximum torque of 1.2 Nm (4 times the zero field torque). The device was tested by moving a cursor through a force field on the computer screen. The author's reported experiencing "strong differences in the resistance force" when moving "the stick in fields of different strengths". They also provide a plot of the measured dependence of torque on electrical field strength.

Due to the geometry of the actuator, a large shearing friction between the two electrodes was experienced.

2.2.2 Cylindrical ER Actuator: Active Device

A series of papers written by Sakaguchi, Furusho, Genda and Zhang [16, 17, 18, 21, 19, 20] discuss haptic systems investigated by them.

Furusho and Sakaguchi(1997) [16] developed a parallel link type force display system, using particle type ER fluids. The actuator was of the cylindrical type and could produce force in two directions. This was achieved by using two input rotational cylinders driven in different directions by a single electric motor and a gearing system. Each input cylinder is connected to its own power supply. Input torque is transmitted to the output rotational axis through the ER fluid. Output torque is controlled by controlling the electrical field between the electrodes. Note that this is an inherently active actuator since energy is fed into the system via the motor. Also, operating the clutch in this mode eliminates the need of having to handle the static shear stress effect of ER fluids, since by having the motor and hence the two input cylinders continuously rotating, only dynamic shear stresses are experienced.

The following findings were reported from experiments carried out on the ER actuator:

- The time constants for the torque response to voltage step inputs of 0.2 kV/mm at 1.0 kV/mm, 1.8 kV/mm and 2.6 kV/mm with this actuator were all found to be between 3-4 ms.

- The resulting magnitude increase in torque at each field strength was found to increase with increasing field, with a step size of 0.2 V/mm.

- Increasing the rotational speed linearly while keeping the voltage on both output electrodes constant was found to have no effect on the output torque.

A parallel link type force display system was constructed utilizing two of the ER actuators discussed above. The device was capable of producing a force of 50 N in a 30 x 50 cm workspace. The following scenarios were simulated using this device:

- Wall: The smooth surface and corner of a virtual wall were felt.
- Push: The sense of pushing a heavy object was felt.
- Viscous Fluid: Different forces were felt by moving the actuator through a viscous field.

The authors conclude by proposing a wire driven force display system which could be utilized for training in surgery.

Detail on the control of the ER actuator is given in a later paper (1998) [17] written by the same authors. Here the authors mention that the linearization of the non-linear properties of the ER fluid have been implemented via computer simulations. "Push-pull" control is also used to produce clockwise and counter clockwise torques. Results for a step response in position using a PID controller are presented.

The authors present results for simulating a two dimensional spring and a force field and a proposal for the use of ER haptic devices in rehabilitation training.

A later paper presented by Sakaguchi, Furusho and Genda [19], details experiments, carried out with the same force display system, in rehabilitation training.

2.2.3 Passive ER Brake

A passive force display system was presented by Sakaguchi, Furusho and Takasue [20] in 2001. The brake design was of the cylindrical electrode type, which is similar to the active clutch discussed in Section 2.2.2. Here however, there is no motor adding energy to the system. The lower cylinder is fixed, while the output cylinder alone is rotational.

The authors present the basic characteristics of the ER brake: dimensions, torque-field profile, shear rate vs. torque characteristics and the step response of the ER brake.

The outside diameter of the rotating cylinder is 108 mm, a gap width of 1 mm is used and the effective surface area is reported as being 264 cm^2. A maximum torque of 0.9 Nm was reported at a field strength of 3 kV/mm. The step input plot presented by the authors indicated a rise time of approximately 10 ms (10% to 90%).

The ER brakes were fitted to a force display system similar to the parallel link mechanism described in Section 2.2.2. The scenarios simulated were a touch and detach wall simulation, the sensation of collision with a virtual object and tracing of a wall surface.

The above scenarios were simulated using logical operators to switch the states of the brakes between 'on' and 'off'. No further detail of the control logic is presented.

2.2.4 Passive Haptic Glove

A haptic glove utilizing ER Dampers is discussed by Mavroidis, Pfeiffer, Celestino and Bar-Cohen [14]. The authors have developed a haptic interface system called MEMICA (remote mechanical mirroring using controlled stiffness and actuators), which is a glove equipped with a series of electrically controlled stiffness(ECS) elements (small ER dampers). They develop a model for the ECS and test this model on a scaled version of the ECS. MEMICA is currently being used in a system to perform virtual tele-surgery.

2.3 Clutches

Much work has been done by Hosseini-Sianaki et al [7] and Johnson et al [9] on high speed ER clutches, mainly for use in the automotive industry.

Johnson et al perform testing on a high speed cylindrical type clutch, and also provide important information on the design of clutches, which is briefly summarized below.

- The clutch has to have a high torque/inertia ratio. Reasons for this requirement is that with a low inertia output member, the speed of response will be as fast as possible when the ER fluid is energized. (They designed their output member to have a moment of inertia of 4 x 10^{-4}kg.m^2.)

- The electrode gap should be as small as possible when compared with the radius.

This is to eliminate radial effects. (They chose a radius of 30 mm with an electrode gap of 0.5 mm.)

The authors used speeds of up to 3000 rpm and reported time constants of 1 ms. The authors also report a fluid degradation problem. Their clutch load pick up times increased by 25 % over the six month period that the fluid was in the clutch. They reported that a rapid fall in the performance occurred over the first few weeks followed by a much slower fall in performance in later weeks. The reason for degradation was undetermined. No information was given on the ER fluid used.

Hosseini-Sianaki et al [7] perform testing on the speed of torque response for various speeds and at various temperatures. Their results for time responses and torques are shown in Table 1 below:

Table 1: Table showing results as presented by Hosseini-Sianaki et al [7].

Temp	23°C		32°C		42°C	
Speed	250 rpm	1000 rpm	250 rpm	1000 rpm	250 rpm	1000 rpm
Response Time (ms)	3.47	2.7	2.6	1.54	1.71	0.98
Torque (Nm x 10^{-3}	10.23	8.85	10.35	9.38	10.43	10.33

Kim, Choi and Cho [12] developed an ER brake actuator to control wire tension on a wire cut discharge machine. A relationship between wire tension and electric field is formulated and this is successfully used to control the wire tension and vibration of the wire in a wire cut machine.

2.4 Modelling and Simulation

Butz and von Stryk [5] present a survey of various modeling techniques used to simulate the nonlinear characteristics of electrorheological fluids. They present a nonlinear visco-elastic plastic model, developed by Kamath and Wereley [11], which accurately models the pre-yield to post-yield transition in electrorheological fluids.

Kamath and Wereley present a nonlinear dynamic model that relates shear strain input to shear stress response. The ER fluid behavior is modeled by dividing the fluid into two rheological domains: pre-yield and post-yield. A shear flow mechanism is used to model

each domain. A nonlinear combination of these mechanisms is then used to predict the pre-yield to post-yield fluid behavior.

It should be noted that most of the work done in the modeling of ER fluids have been done for the application of ER fluids in dampers.

2.5 Summation of Literature Search

Even though much research has been conducted on ER fluid behavior in general, not much work has been done in the area of passive ER braking devices for haptic systems. Furusho and Sakaguchi [20] have developed a passive system however they do not discuss much experimental work. Questions that need to be answered are:

- How is the static and dynamic effect of yield accounted for?
- What effect does this static and dynamic yield have on the braking torque?
- What are the yielding characteristics of ER fluids at low shear rates?

Bose and Berkemeir [3], fell short in the design of their passive haptic clutch, in that the frictional elements of their clutch were too large.

A need for developing a design methodology as well as more experimental work in the use of ER fluids in passive braking devices definitely exists.

CHAPTER III

EXPERIMENT REQUIREMENTS

3.1 Motivation for Experimental Work

From the literature survey it should be quite clear that only two other researchers, Bose et al [3] and Furusho et al [20] have used ER braking systems in passive haptic interfaces. Other previously published testing and information on the use of ER fluids in clutches, focus on high speed systems, mainly for use in the automotive industry. The use of ER fluids in passive braking devices is therefore still in the infancy stages and much work needs to be done in this area.

The focus of this project was consequently directed towards the designing of passive ER brakes, building a test bed based on the design methodology developed, determining the fundamental characteristics of the designed brake at low operating speeds and evaluating the success of the design by comparing test data with theory and available literature.

3.2 Designing with ER Fluids

Designing with ER fluids requires a holistic approach. A component in an existing system cannot be removed and replaced by an ER device, instead the design of the entire system has to be based around the ER device. According to Brooks [4] five basic elements are involved in the design of ER systems. These are the ER mechanical component, the ER fluid, the high voltage source, the controlling logic circuit and the feedback element. All these elements are shown in Figure 10.

The mechanical element refers to the device being designed. This could either be a clutch, a brake, a valve or any other device utilizing ER fluids. The design process for designing a complete ER braking device will be presented here.

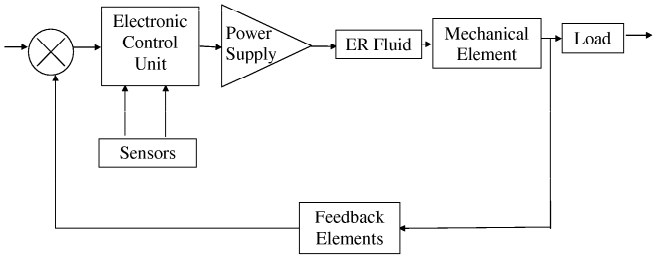

Figure 10: Block diagram of a typical ER system layout Brooks [4].

3.3 Fluid Selection

The most important aspect of designing with ER fluids is the selection of the ER fluid. Properties that the ideal ER fluid need to possess are:

- Fast response times
- Small zero field viscosity
- Minimal settling
- Consistent mechanical properties over a wide temperature range.
- Good dielectric properties
- Non-toxic
- Low power requirements
- Non-corrosive
- Non-abrasive
- Low cost

Unfortunately, engineering catalogue information on ER fluids do not exist. Most ER fluids used in previously published research, were either manufactured by the researchers themselves or were developmental fluids provided to the researchers for testing.

An extensive search for commercially available ER fluids was conducted. Company names were obtained from previously published research papers, researchers who had previously worked with ER fluids and various internet sources. The most extensive source of information was an internet site maintained by Lampe [13]. This was a database of commercially available ER fluids and their property comparison.

From the abovementioned searches, companies contacted included: Lord Corporation, Nippon Shokubai Co. Ltd., Asahi Chemical Company, Bridge-stone Firestone, ER Fluid Developments Ltd. and Bayer. Of these companies all except ER Fluid Developments Ltd. (ERFD) had stopped manufacturing and supplying ER fluids commercially. Since ERFD was the only available supplier of ER fluids, the fluid used in the current research was purchased from them.

Thus a choice in the type or properties of the ER fluid purchased was not possible and the only commercially available fluid was purchased.

Data sheets of the fluid purchased are presented in Appendix A.

3.4 Design Methodology

The design methodology presented here is specifically for cylindrical clutch type ER brakes, type (b) in Figure 8. This design methodology however can be modified to suit various clutch geometries.

The cylindrical clutch geometry is reproduced here, in Figure 11, with the necessary geometric design parameters highlighted.

In this arrangement it was assumed that the outer cylinder is stationary while the inner cylinder rotates at an instantaneous speed, Ω. The inner cylinder radius is denoted as R_1, the outer cylinder radius as R_2 and the length of the cylinder as L. It is also assumed that high voltage is applied to the stationary electrode while the rotating electrode is grounded.

The first step in the design process was to determine the output torque that was required

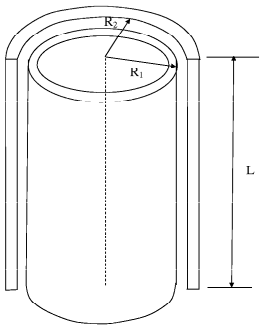

Figure 11: Geometric design parameters of a cylindrical ER clutch.

to be produced by the ER clutch. From Equation 15, the total torque output of an ER brake is composed of two components, the torque due to electrical field and the torque due to speed. The torque due to electrical field is dependent on:

- Electrode Gap Width
- Electrode Surface Area
- Electrical Field

Electrode gap width is defined as:

$$h = R_2 - R_1 \tag{17}$$

while electrode surface area can be written as:

$$A = 2\pi R_1 L \tag{18}$$

(L is the effective length of the electrodes as shown in Figure 11.)

Electric field is given in Equation 11, and repeated here with r replaced by R_1.

$$E = \frac{V}{ln(\frac{R_2}{R_1})}\frac{1}{R_1} \tag{19}$$

A quick browse through Equations 17 - 19 reveals that the torque due to field is a function of R_1, R_2, L and V. Changing any of these parameters would change T_y. Equations 17 - 19 were combined to form one equation for for yield torque, Equation 20.

$$T_y = 2\pi\alpha l\left(\frac{V}{ln(\frac{R_2}{R_1})}\right)^2 \tag{20}$$

Here α is an ER fluid constant, that should be supplied by the manufacturer of the fluid. Equation 20 was used to develop a spread sheet that calculates T_y at various radii, lengths and voltages, and outputs a graph featuring these characteristics. From this graph it is possible to pick the required value for T_y and then determine the physical size of the clutch and the voltages at which these torques are achievable. A sample output of this spreadsheet is shown in Table 2. The geometry ratio here is simply the ratio of R_2 to R_1, while the effective voltage is the actual voltage divided by the natural logarithm of the geometric ratio.

Table 2: Table showing a sample of calculated design data for T_y from the programmed spread sheet.

T_y (Nm)	Inner Radius (m)	Outer Radius (m)	Geometry Ratio	Voltage (V)	Effective Voltage (V)
7.841834129	0.039	0.04	1.025641026	4000	157991.5608
8.243957989	0.04	0.041	1.025	4000	161991.7692
8.656134946	0.041	0.042	1.024390244	4000	165991.9676
9.078364999	0.042	0.043	1.023809524	4000	169992.1566
9.510648149	0.043	0.044	1.023255814	4000	173992.3369
9.952984395	0.044	0.045	1.022727273	4000	177992.5091
10.40537374	0.045	0.046	1.022222222	4000	181992.6738
10.86781618	0.046	0.047	1.02173913	4000	185992.8313
11.34031171	0.047	0.048	1.021276596	4000	189992.9822
11.82286034	0.048	0.049	1.020833333	4000	193993.127
12.31546207	0.049	0.05	1.020408163	4000	197993.2658
12.8181169	0.05	0.051	1.02	4000	201993.3992
13.33082482	0.051	0.052	1.019607843	4000	205993.5273
13.85358584	0.052	0.053	1.019230769	4000	209993.6506
14.38639995	0.053	0.054	1.018867925	4000	213993.7693
14.92926716	0.054	0.055	1.018518519	4000	217993.8837

In Table 2, only calculations at a voltage of 4 kV is shown. It would be too cumbersome to present all the data, however, a graphical representation of all data that was generated is shown in Figure 12.

The corresponding values for α, L and h used to generate the data in Table 2 are shown in Table 3. Note that α is an ER fluid constant provided by the manufacturer.

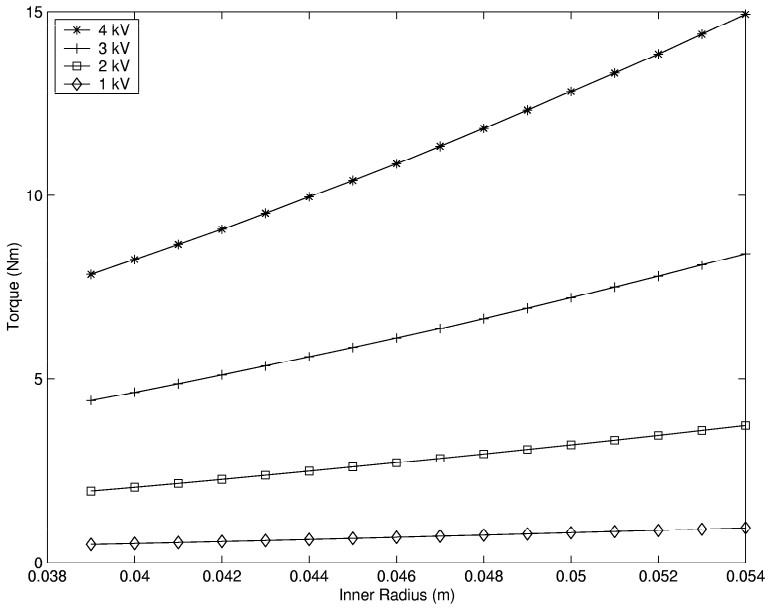

Figure 12: Graphical representation of data presented in Table 2.

Table 3: Table showing the values used of α, L and h used to generate data for Table 2.

α	2.5E-10	$\mathrm{Pa/(V/m)^2}$
l	0.2	m
h	0.001	m

Table 2 and Figure 12 can be used to see effect of changing a particular parameter. If for instance, it was necessary to see the effect of halving the electrode area by decreasing L to 0.1 m, then this parameter can be changed in the spread sheet and the outcome of this change is shown in Figure 13.

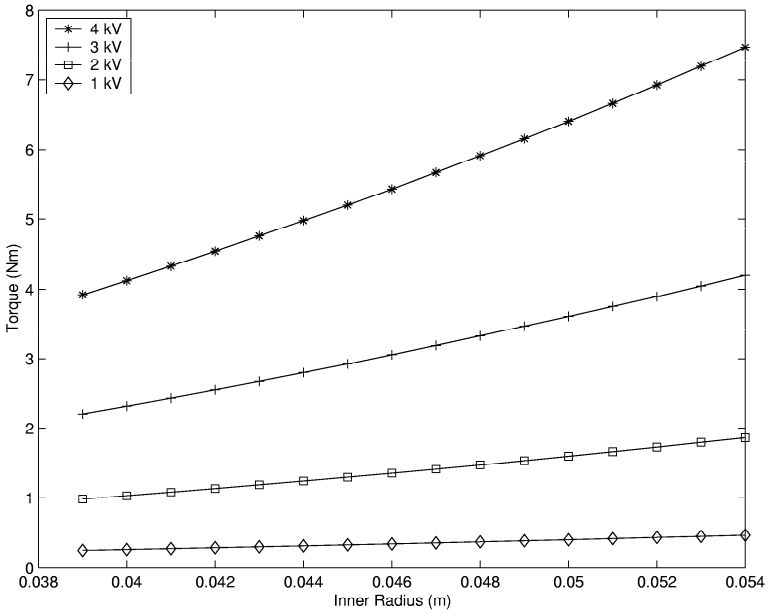

Figure 13: Effect of halving electrode area by decreasing L to 0.1m

Like-wise similar torque plots can be generated for various radii as well as different electrode gap widths.

Up until now, only the calculation of one component of the total generated torque has been discussed. The torque component due to velocity still needs to be calculated. The component of torque due to velocity, T_ω, can be written as:

$$T_\omega = \frac{4\pi\eta_{pl}\Omega l R_1^2 R_2^2}{R_2^2 - R_1^2} \tag{21}$$

The plastic viscosity, η_{pl}, in this equation is assumed to be constant, however, in reality this is not always the case and η_{pl} usually varies with field strength. This torque component is dependant on the geometric parameters, R_1, R_2 and L, and the operating speed of the device, Ω.

It was decided that by first choosing the geometric parameters, and then evaluating the torque due to speed of rotation, more manageable chunks of data would be obtained. The

geometric parameters were therefore first chosen from Table 2 and Figure 12.

A similar spread sheet, to that shown in Table 2, was then constructed, to calculate T_y and ultimately the total torque. The output from this spread sheet is shown in Table 4.

Table 4: Table showing the generated values of T_ω

Speed (rpm)	Angular Velocity (rad/s)	Velocity Component Torque (Nm)
0.25	0.026179939	8.27E-04
0.5	0.052359878	1.65E-03
0.75	0.078539816	2.48E-03
1	0.104719755	3.31E-03
1.25	0.130899694	4.13E-03
1.5	0.157079633	4.96E-03
1.75	0.183259571	5.79E-03
2	0.20943951	6.61E-03

Using the torque values generated in this Table, total torque was then calculated for each speed and voltage. A typical graphical output from the data generated in this calculation is shown in Figure 14. The speeds in these calculations range between 0.2 rpm and 2 rpm.

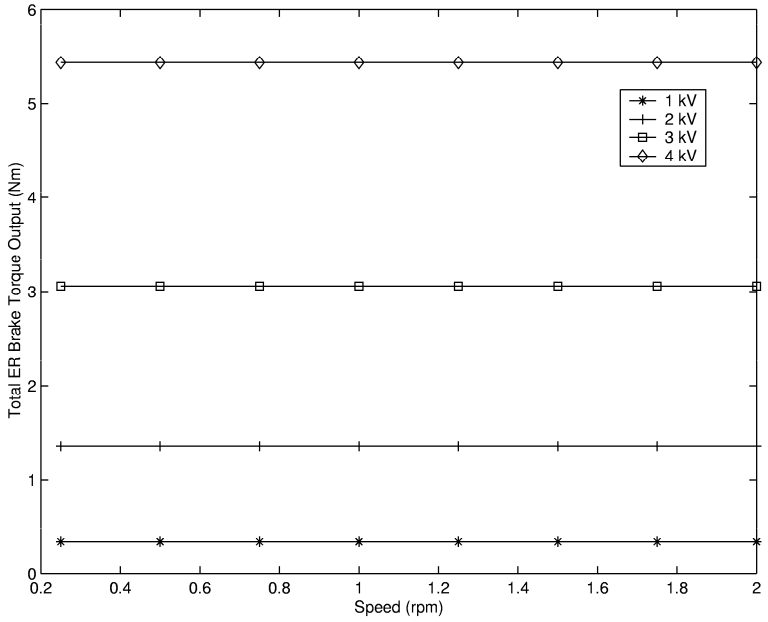

Figure 14: Total torque output graph generated by the simualtion.

At these speeds the torque remains constant over the entire range of speeds chosen. If it was required to see the effect of using faster speed, the required speed values can be entered

into the spread sheet and the relevant torques calculated.

Figure 15 shows the effect of using larger speeds (from 500 rpm to 4000 rpm) on the total torque output of the clutch. From this Figure it can be seen that speed does have a considerable effect on output torque when a wider range of speed is considered. One more

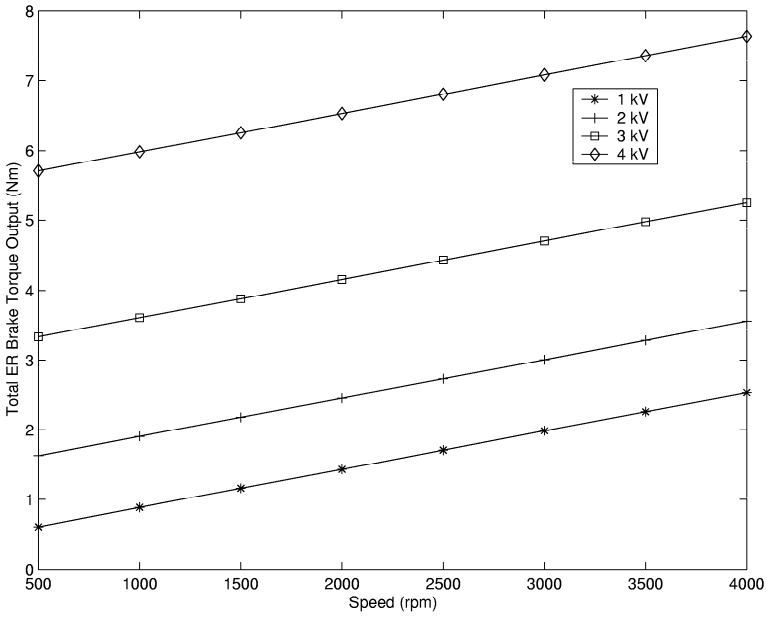

Figure 15: Simulated effect of increasing speed on the total torque output.

useful graphical output can be obtained from these spreadsheets: the torque voltage profile. A typical torque voltage profile is shown in Figure 16. This Figure shows that torque follows a parabolic profile with voltage.

3.5 Design of Test Equipment

The methodology presented in section 3.4 was used to design the test equipment used in the current research. The following requirements had to be adhered to when designing the clutch:

- To achieve a constant field strength across the electrode gap i.e. to reduce radial effects on electric field strength, the radius of the inner cylinder R_1 has to be large in comparison with the gap width.

- The design had to have a large torque to inertia ratio. This implied that the inertia

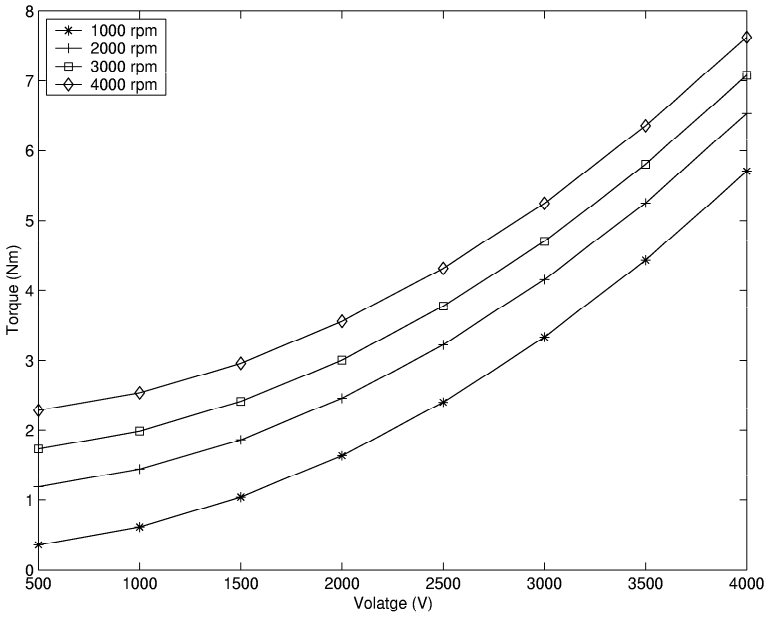

Figure 16: Relationship between total torque output and voltage at various speeds.

of the output member had to be kept as small as possible.

- The clutch was required to provide an output torque of 5 Nm at 4 kV.

Based on these requirements a cylindrical clutch type ER brake design was selected because a larger torque to inertia ratio was possible with this geometry.

3.5.1 Determination of Size of Electrodes

Based on these requirements, the effects on yield torque using various radii for the inner electrode, were simulated in the spread sheet. For ease of manufacture, and to allow for any vertical misalignment that may be present, a conservative gap width was chosen. It was found that at an inner electrode radius of 45 mm, a gap width of 1 mm and a cylinder length of 0.1m, a yield torque of just over 5 Nm was achievable. This is shown in Figure 17. These parameters yield a ratio for R to h of 45, which was considered to be sufficiently large to maintain a constant field strength across the gap.

The choice of dimensions were also affected by the availability of off the shelf aluminum round bar and tubes.

Based on these dimensions, the total torque vs. speed characteristics were simulated for

small speeds of up to 60 rpm. The result of this simulation is shown in Figure 18. From this figure it is apparent the maximum torque that can be produced by the chosen electrode size is 5.467 Nm at a voltage of 4 kV.

Since torque remains approximately constant over the entire speed range under consideration, only curves for speeds of 10 rpm and 60 rpm were plotted. Only 'one' curve is apparent in Figure 19, so it can be deduced that speed will not have an effect on output torque, in the speed range under consideration.

3.5.2 Design of Brake

The next step in the design process was to package the electrodes into a suitable braking system. Here the moment of inertia of the output system had to be made as small as possible to maximize the torque to inertia ratio. A 2 mm thick, aluminum sleeve was used to line the inside of a delrin cup. Aluminum was chosen as the material for the electrodes because of its high strength to weight ratio and good conductivity.

The purpose of the delrin was two-fold: to reduce the inertia of the output and to insulate the high voltage electrode. Figure 20 shows a drawing of the delrin cup and Figure 21 shows a drawing of the outer electrode.

The inertia of the outer electrode about the axis of rotation was 4.0809 x 10^{-4} kg.m^2 and that of the delrin cup was found to be 0.0026 kg.m^2. The total inertia of the output side was therefore 0.0030 kg.m^2. This results in a maximum torque to inertia ratio of 1.8333 *10^3 N.m/kg.m^2. This was deemed to be sufficiently large for the current experimental purposes.

The inner electrode and the input shaft of the device was designed to be the same. This was the grounded electrode, so there was no danger of exposing any electrical components, which were coupled to this shaft, to high voltages. This feature also kept the design of the device simple. Figure 22 shows a drawing of the inner electrode.

The shaft was supported in a housing by two angular contact ball bearings. A carbon brush fitted in the housing of the brake, in-between the two bearings, provided a grounding contact for the shaft. (The inertia of the input shaft was not a critical aspect of the design.)

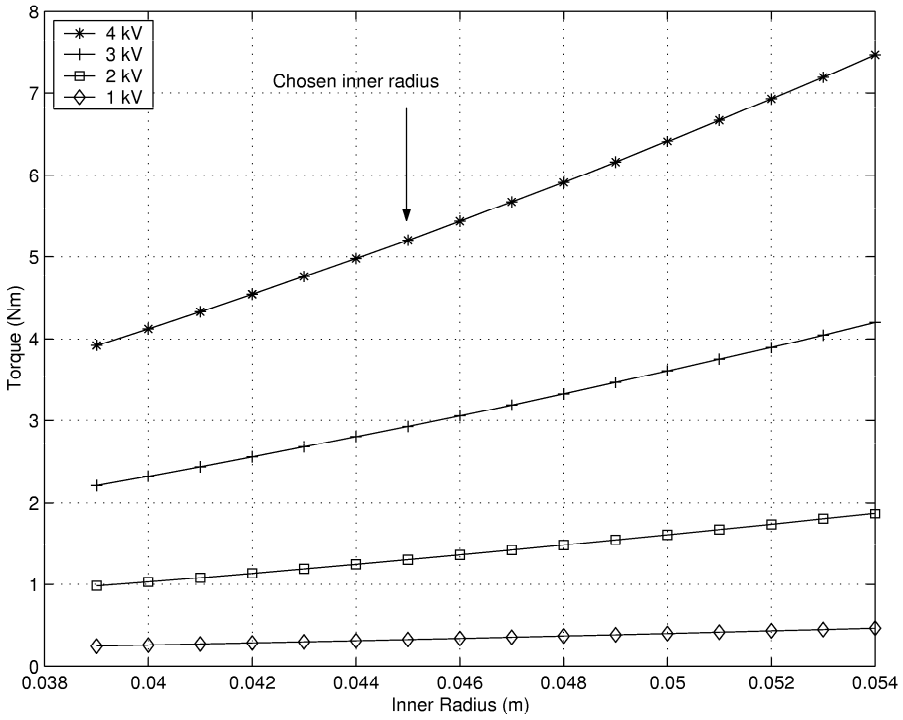

Figure 17: Chart used to select the size of the inner electrode.

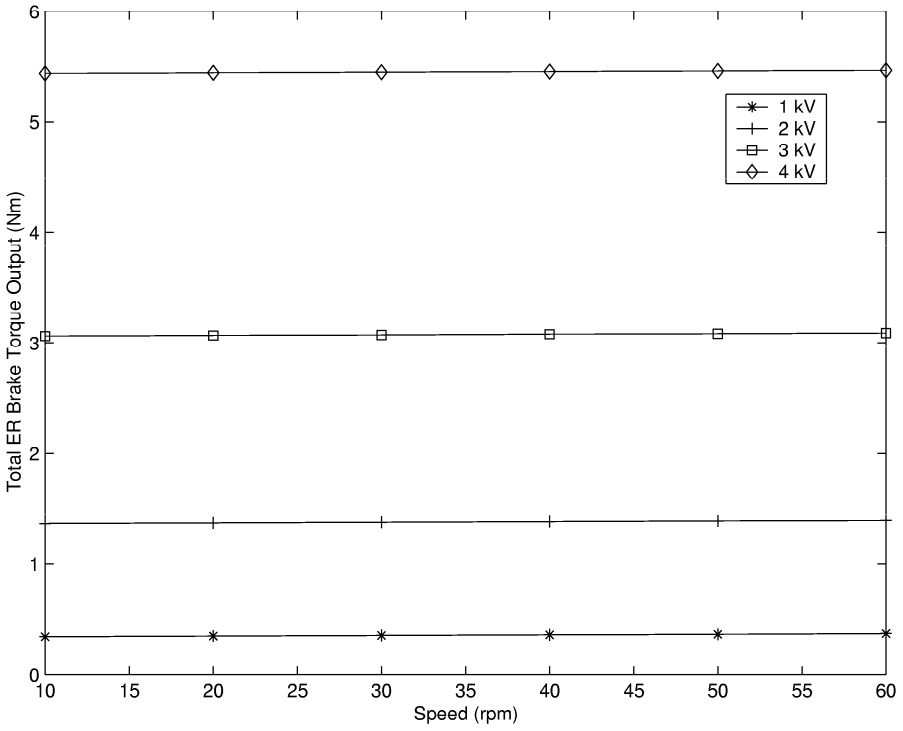

Figure 18: Simulated torque vs. speed characteristics of the test equipment.

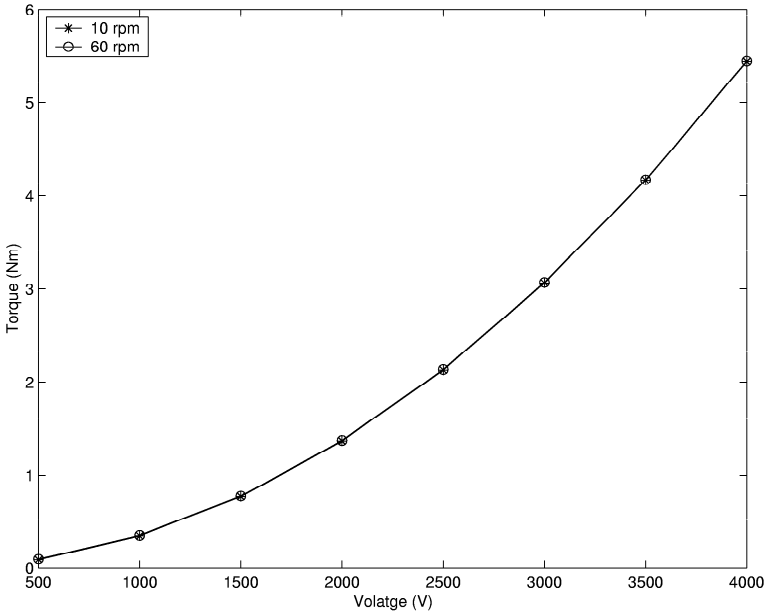

Figure 19: Simulated torque vs. voltage characteristics of the test equipment.

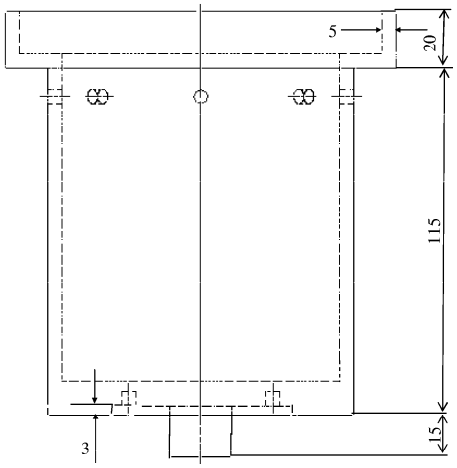

Figure 20: Drawing of the delrin cup used to insulate the outer electrode.

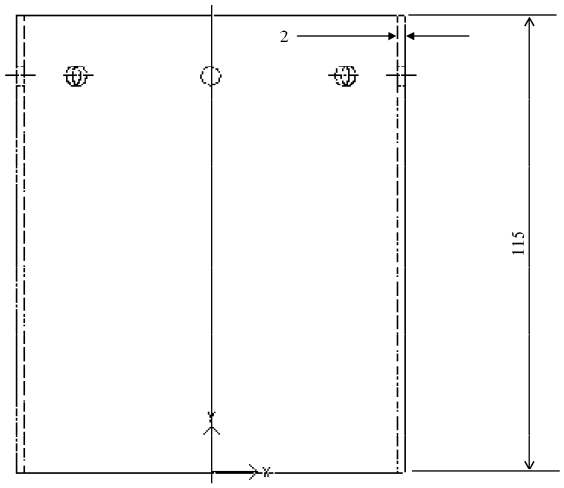

Figure 21: The outer electrode made from a 2 mm thick aluminum sleeve.

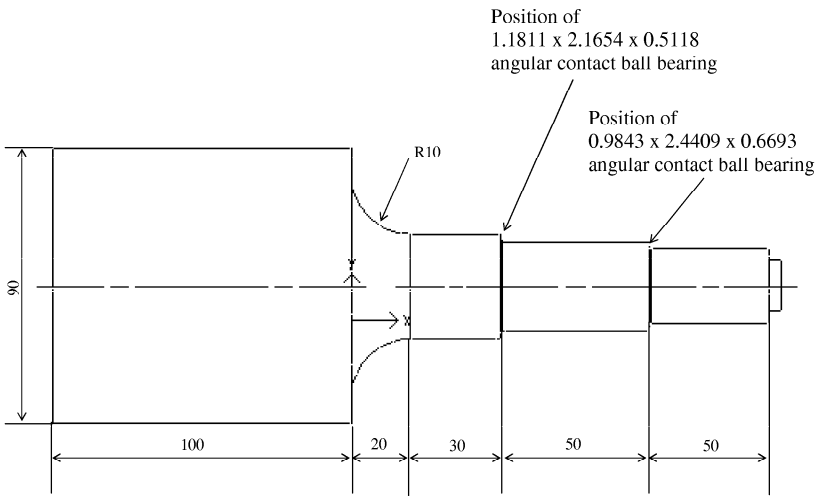

Figure 22: The inner electrode, which doubled as the input shaft.

The shaft was coupled to an electric servo motor via a harmonic drive. The delrin cup was fixed to a rotary reaction torque sensor which in turn was fixed to the base of the housing. Figure 23 shows a drawing of the general arrangement of the entire device.

The housing was manufactured out of one solid piece of aluminum round bar. This ensured that the shaft was well aligned and positioned in the delrin cup assembly. The entire assembly sat on a square base plate which had alignment grooves for the positioning of the housing and the torque sensor.

A handle was designed and manufactured to couple directly onto the shaft so that simple haptic experiments could be carried out. Figure 25 shows an arrangement with the handle. The test apparatus used in this configuration would be able to simulate a one degree of freedom haptic system. The attachment at the top of the handle is a rotary optical encoder for position and velocity feedback.

3.5.3 Power Supply Requirement

One of the main constraints in the design process of ER brakes is the size of the power supply. The two factors governing the size of the power supply are the ER fluid and the effective electrode area. The ER fluid determines the current density requirements. Using the effective electrode surface area, current requirements can quite easily be calculated. Here the manufacturer's catalogue information on the ER fluid, was used to determine the power supply requirements. However discrepancies did exist between the information used and the actual data for the particular batch of fluid supplied for the current use. First the actual process that was used in the selection of the power supply will be discussed. The error in this calculation will be then discussed .

Figure 29 in Section 4.1 shows the current density requirements for the ER fluid used. At a field of 4 kV/mm, a current density of approximately 11.2 μ A/cm^2 is needed. Based on the dimensions specified in Section 3.5.1, it was found that the required current at a field of 4 kV/mm is 3.2 mA. The power supply would therefore need to produce a current of 3.2 mA at a voltage of roughly 4 kV.

The Batch data, however that was supplied by the manufacturer and which is shown in

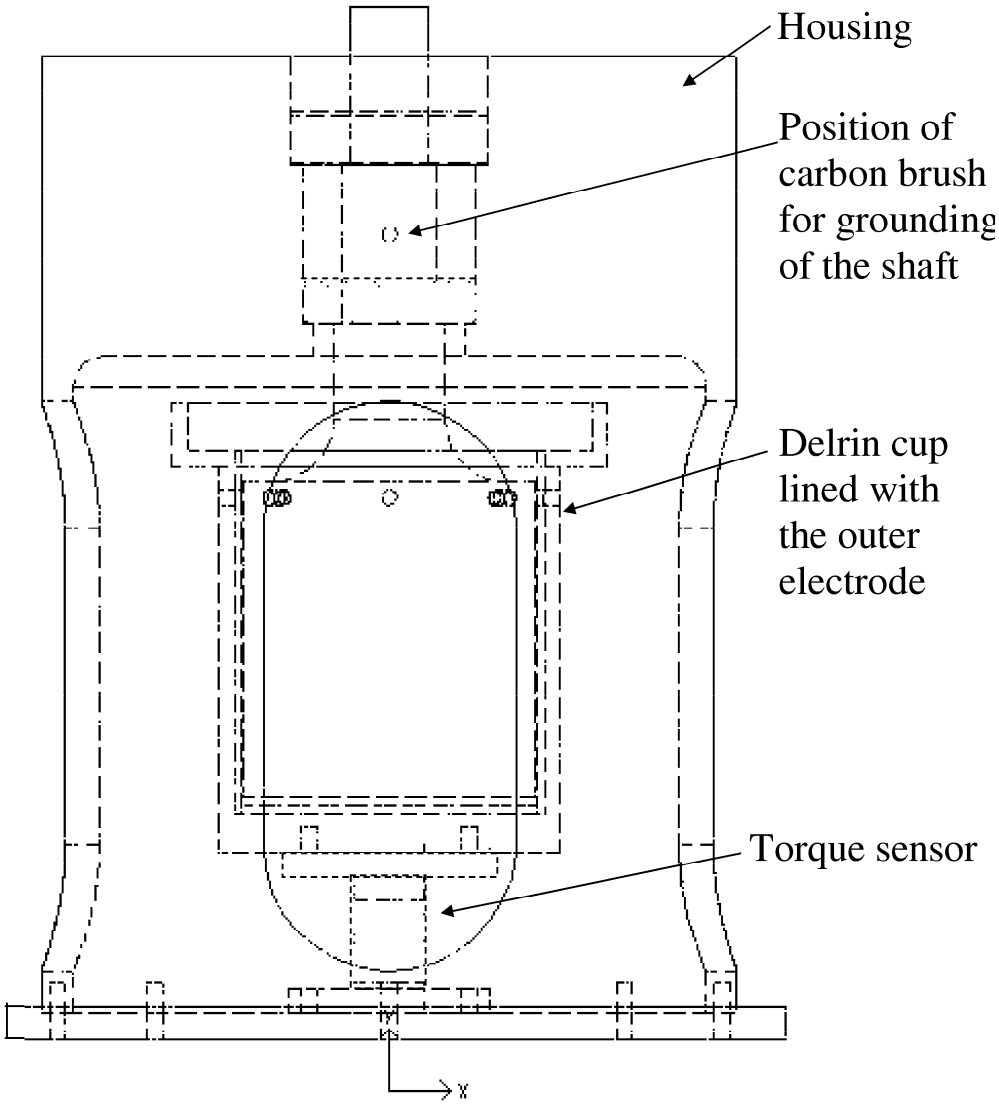

Figure 23: Assembly drawing of the inner electrode, the outer electrode, the delrin cup and the torque sensor in the brake housing.

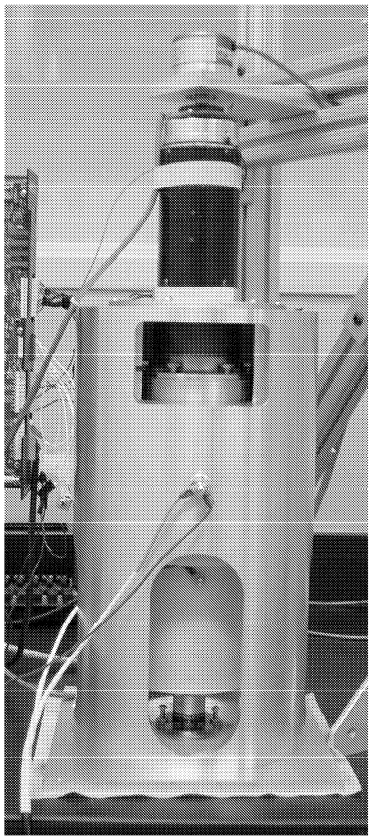

Figure 24: Photograph of the designed braking device in the housing.

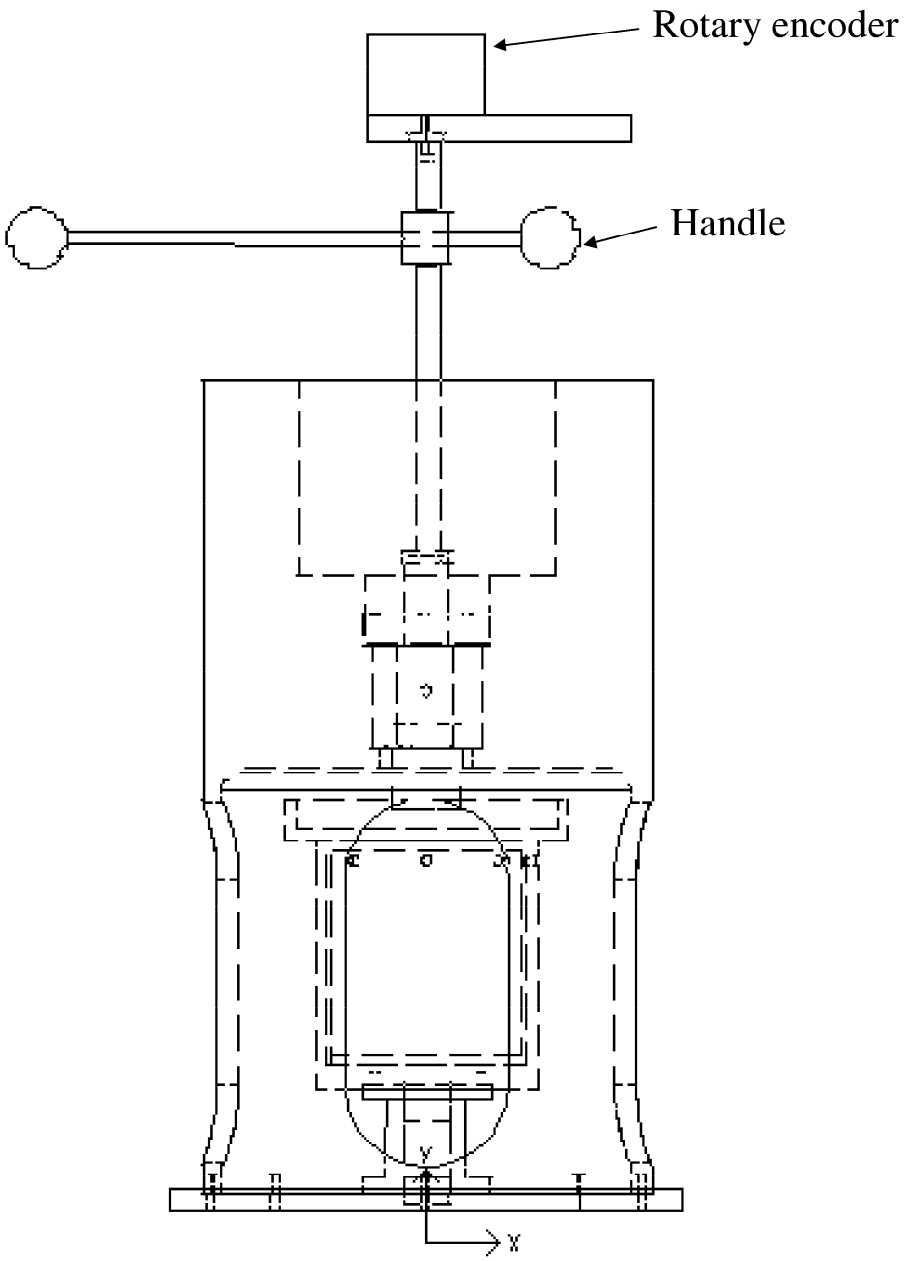

Figure 25: Drawing of the brake with the handle attachment.

Table 6, indicates that the current density at a field strength of 4 kV/mm, is 21.0 μ A/cm^2. This results in a current requirement of approximately 6 mA at 4 kV/mm. The power supply used in this research was therefore under designed and thus usable voltage was limited to 2.5 kV.

3.6 Torque Sensor Selection

The torque sensor that was chosen had to have a high stiffness. The stiffness of the torque sensor used was 19372.2 Nm/rad. Together with the inertia of the output, the transfer function was found to be: $G(s) = \frac{1}{0.003s^2+19372.2}$. The frequency response of this transfer function is shown in Figure 26. Based on this frequency response it was decided that the stiffness of the torque sensor was adequate for measuring the response of the ER brake.

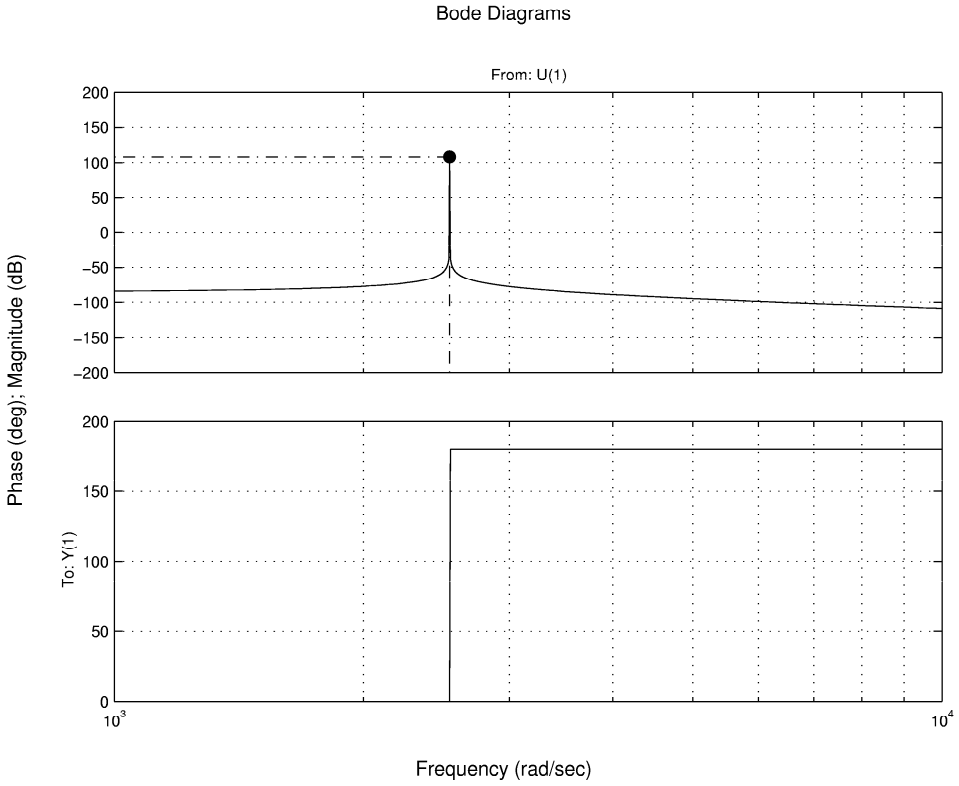

Figure 26: Frequency and phase characteristics of the output system.

CHAPTER IV

TESTING

4.1 Hardware and Software Setup

A schematic of the general set up is shown in Figure 27 while a photograph is shown in Figure 28.

A Heimmelstein Company RTM 2020(24-1) Hollow Reaction torque sensor was used to measure the torque. The torque transducer has a full foil gauge torque bridge sensor and gives an output of 1 mV/V up to 10 mV with an excitation of 10 V. The signal from the torque transducer was conditioned using an ANALOG DEVICES 3B18 signal conditioning system. The 3B18 provide 10 V bridge excitation and can accept a strain gage input of up to 20 kHz bandwidth.

A Bertan Series 230-05R high voltage power supply was used. This power supply was capable of producing a maximum voltage of 5 kV with a current output of 3.0 mA. The maximum current output was limited to 120% of this value so effectively a current of up to 3.6 mA could be supplied. The voltage level on this power supply could be remotely controlled with 0 to +5 V dc signal which proportionally produced a 0 to 5 kV output. The short circuit current is limited, arc protected and self-restoring. Two 0 to +5 V outputs, which were proportional to 0 to maximum current and voltage were also available for remote current and voltage monitoring.

An IMEC 400 Series SC402-001 controller was used to control the Pacific Scientific Brushless DC motor. The controller was set to operate in torque block mode. Since the motor was not fitted with a tachometer, speed had to be monitored separately. This was done using a Lucas Ledex rotary encoder, which had a resolution of 1024 counts per revolution.

A dSPACE DS1102 floating point controller board was used for data acquisition and to control experiments. The board has a built in incremental encoder interface, together

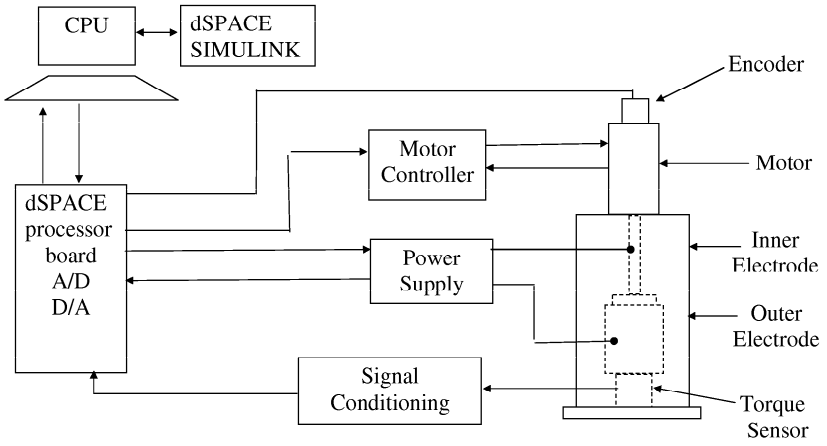

Figure 27: Schematic of the general layout of the experimental setup.

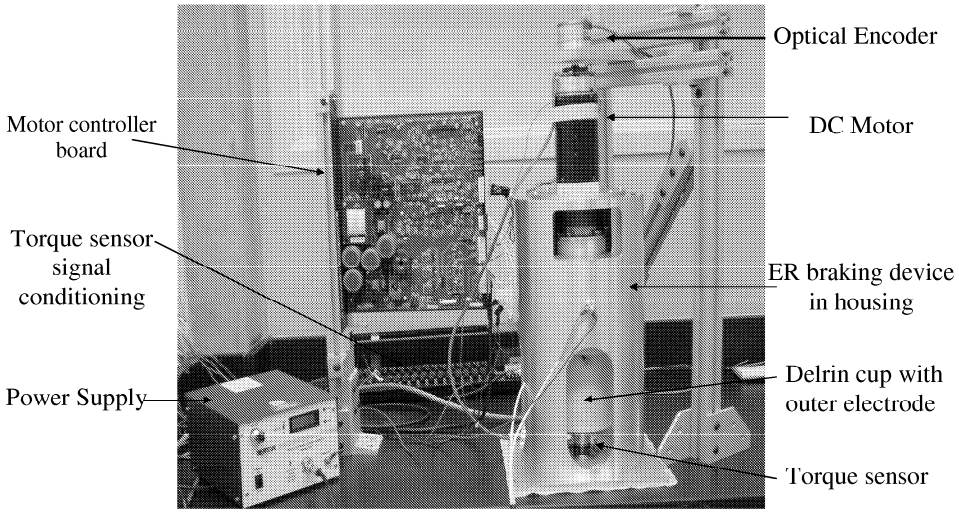

Figure 28: Photograph of the experimental setup.

with 4 analogue inputs and outputs. Channels 1 and 2 of the A/D subsystem have 16 bit resolutions while the remaining A/D as well as all the D/A channels have 12 bit resolutions.

The ER fluid used in the current research can also be classified as a 'hardware' component of the experimental setup. The ER fluid used was LID 3354 made up of 30% volume fraction of polymer particles in a fluorosilicon base oil.

The physical properties are summarized in the Table 5 below, while actual data sheets are provided in Appendix A.

Table 5: Table showing ER fluid LID 3354 properties at 30 °C as supplied by the manufacturer ER Fluid Developments.

Density (kg/m^3)	1.46 x 10^3
Viscosity (mPa.sec)	125
Boiling Point (°C)	>200
Flash Point(°C)	> 150
Freezing Point (°C)	< -20

Static yield stress, dynamic yield stress, plastic viscosity and current density data was also provided by the manufacturer. These are presented in Figure 29.

A separate set of data, containing batch specific, information was provided with the fluid. This information is summarized in Table 6 below.

Table 6: Table showing batch specific data for the ER fluid as supplied by the manufacturer, ER Fluid Developments.

Field kV/mm	Yield Stress kPa	Current Density μA/cm^2	Plastic Viscosity mPa.s
0	0	0	83
0.8	0.35	0.5	49
1.2	0.064	1.4	69
1.6	0.92	2.9	59
2.0	1.34	5.0	-23
2.4	2.09	7.5	-93
2.8	2.32	10.0	-121
3.2	2.84	13.0	-187
3.6	3.50	16.0	-265
4.0	4.18	21.0	-391

The software used was MATLAB, SIMULINK and dSPACE Control Desk. MATLAB and SIMULINK were used to build models. SIMULINK models were compiled and downloaded to the processor. The dSPACE control desk environment was then used to start and

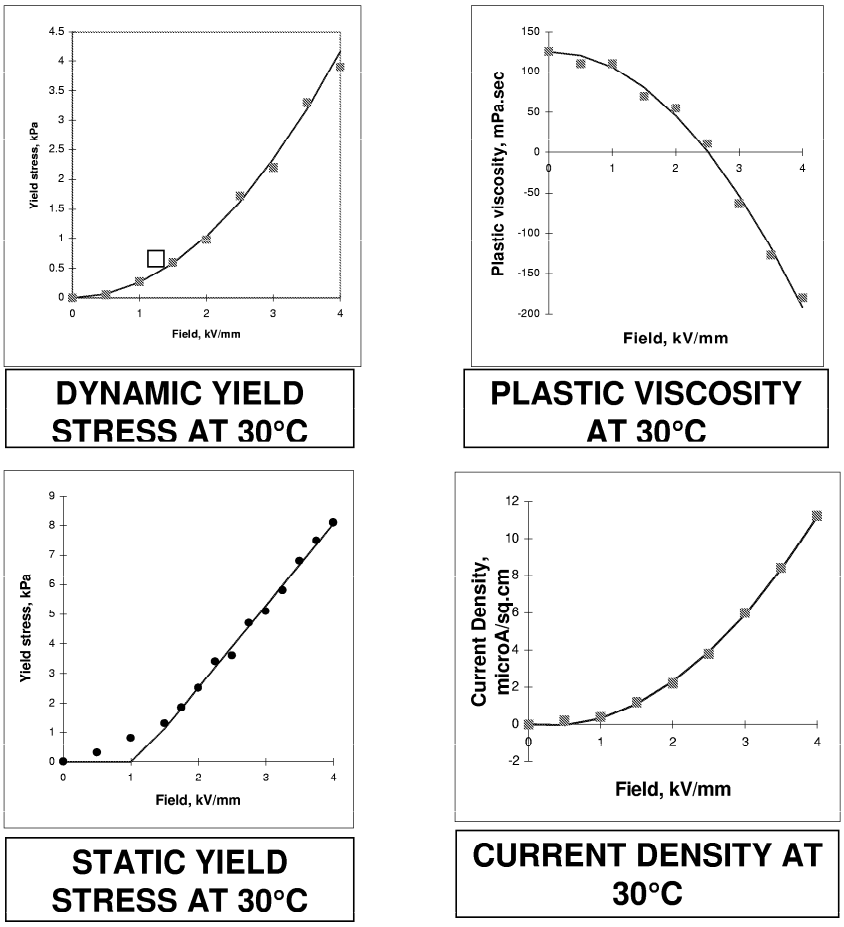

Figure 29: Plots of static yield stress, dynamic yield stress, plastic viscosity and current density of ER fluid LID 3354 as supplied by the manufacturer, ER Fluid Developments.

stop experiments, monitor variables in real time and set sampling rates. Data files were then converted to MATLAB compatible files and all data was analyzed in MATLAB.

4.2 Torque Characteristic of ER Brake

The following information for the clutch system was required:

- Torque Voltage Characteristics
- Static and Dynamic Torque Characteristics
- Torque Velocity Characteristics
- Torque Position Characteristics

4.2.1 Torque Voltage Characteristics

Voltage is used to specify input torque for torque feedback control, therefore a torque-voltage 'calibration' curve of the ER brake is needed. An equation relating torque to voltage is usually presented in literature as being: $T = \gamma E + \alpha E^{\beta}$ where the parameters for γ, α and β have to be experimentally determined.

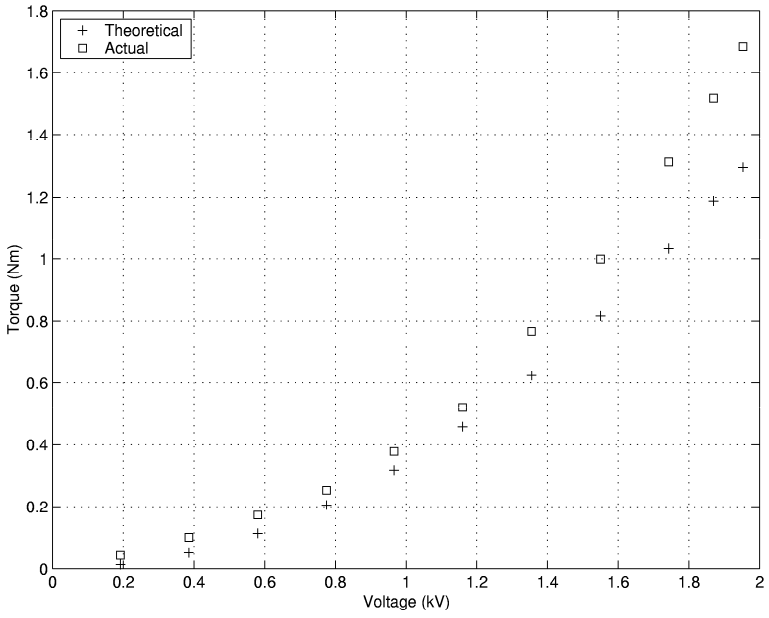

Figure 30: Graph of the actual and theoretical dynamic torque values for the ER brake.

Figure 30 shows a plot of averaged experimental and theoretical torque-voltage values. The data in Figure 30 was obtained by commanding a constant voltage from the power supply while controlling the motor at a set speed. Torque was then measured over a period of 20 s with a sampling frequency of 50 Hz. This was repeated over the entire voltage range. The measured torque was averaged over the measurement period and this value was recorded as the yield stress. Several of these tests were conducted and results were averaged.

Experimental values at each voltage level are higher than that predicted by theory. A possible reason for this variation is that plastic viscosity was assumed to be constant across the range of applied voltages, however in reality this is not the case, as was shown in Figure 29. Another possible reason is that the Bingham model used in the design process is an approximate model. It does not take effects like temperature etc. into account.

Another observation is that experimental data follow the same shape as the theoretical data indicating that even though the model used is not 100 % accurate, it gives a good representation of the characteristics of the actual system.

A quadratic polynomial fit was performed on the data in Figure 30. This is shown in Figure 31. From these results the curve for the torque- voltage profile was approximated as shown in Equation 22:

$$T_d = 0.5227E^2 - 0.2135E + 0.0932 \tag{22}$$

This equation can be used relate commanded torque to voltage in a control system.

4.2.2 Static and Dynamic Torque Characteristics

ER fluids exhibit Coulomb friction type behavior: a certain threshold static torque has to be overcome first before motion commences. The static torque was measured in order to evaluate how it would affect passive haptic systems, since stick-slip, which is felt during the transition between static and dynamic torque, is highly undesirable.

Figure 32 shows static and dynamic values measured for the ER clutch. Here, the required voltage was first commanded from the power supply. Motor speed was then controlled to follow a ramp input and the resulting torque was measured. Static torque was measured at the point at which motion commenced. This test was repeated a number of

times at each voltage level. The average measured static torque with a fitted curve is shown in Figure 32. This average torque is shown together with other static torque runs in Figure 33.

An interesting point to note is that static torque has a quadratic relationship with voltage. A curve fitted to the average static data points yields Equation 23.

$$T_s = 0.2996E^2 + 0.2784E - 0.01438 \tag{23}$$

Figure 33 shows that static measurement data are repeatable. If this holds under various operating conditions then control of the haptic device through the transition between static and dynamic torque would be possible.

4.2.3 Torque Velocity and Torque Position Characteristics

The changes in torque due to position and velocity changes were recorded from the ramp tests discussed above. Results for these tests are shown in Figures 34 and 35.

Figure 34 shows that the torque remains approximately constant over the range of velocities shown. Haptic devices are generally low speed devices so determining the characteristics over this range of speeds was considered to be acceptable. Torque almost looks as if it is independent of speed. This however is not the case. Recall that the torque equation for ER clutches, Equation 15, was composed of two parts, a torque component due to speed and a torque component due to electrical field. The torque component due to velocity in most cases is so small that it's effect is negligible, especially in this case where only slow shear rates have been considered.

Figure 35 shows the torque variation with position. The three regions that ER fluids function in are clearly visible here. Just after time equals zero, the torque increases linearly with position. This region is the pre-yield region where the ER fluid exhibits elastic behavior. As position increases, the torque peaks and usually yielding is assumed to occur at the position at which the torque peaks. Note that yielding occurs at almost the same angular position at each voltage level. (The only exception being at 2.2 kV where yielding has occurred at a much larger strain.) Once the fluid has yielded, torque remains approximately

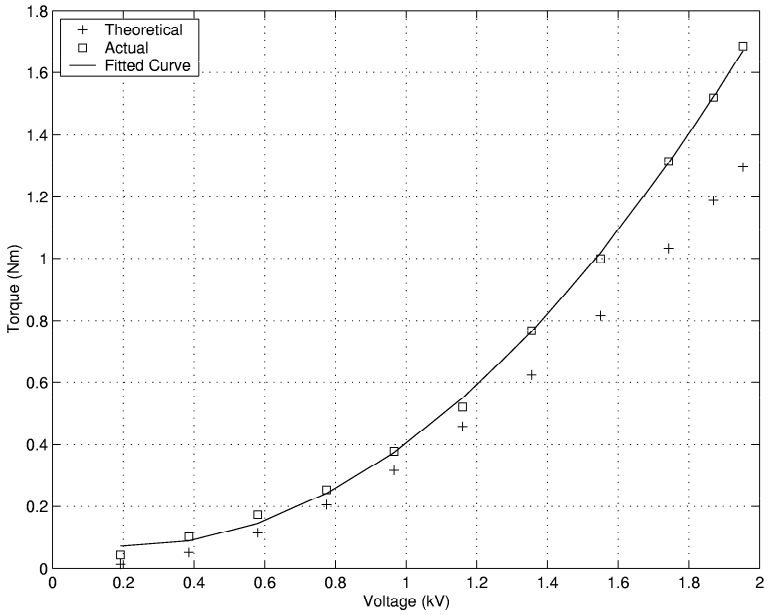

Figure 31: Figure showing measured torque data and the corresponding fitted curve.

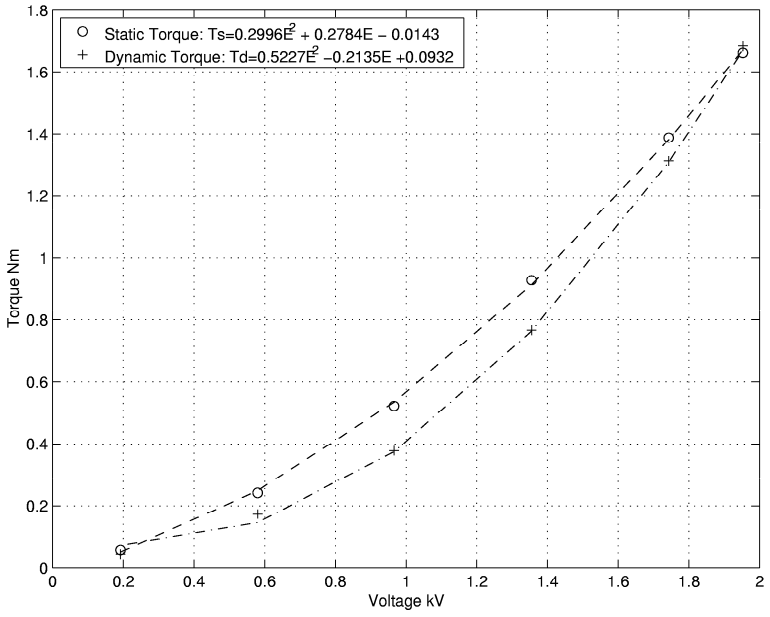

Figure 32: Figure showing the static and dynamic torques measured, together with fitted data.

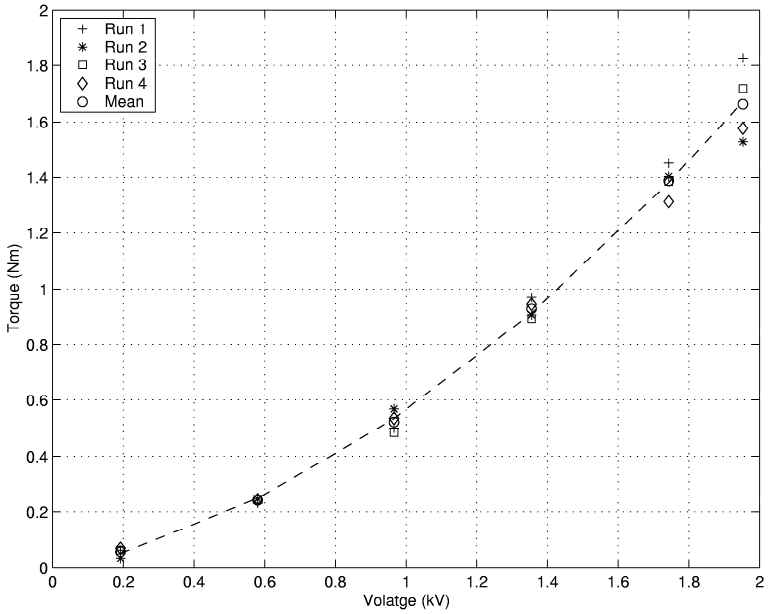

Figure 33: Figure showing different static torque measurements, together with the average measured static torque values and the corresponding fitted curve: Equation 23.

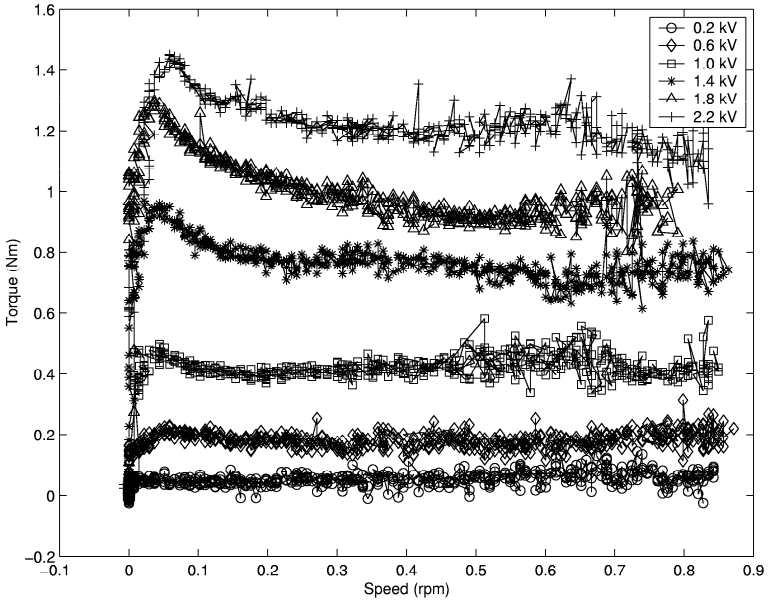

Figure 34: Relationship between torque and speed for ER brake.

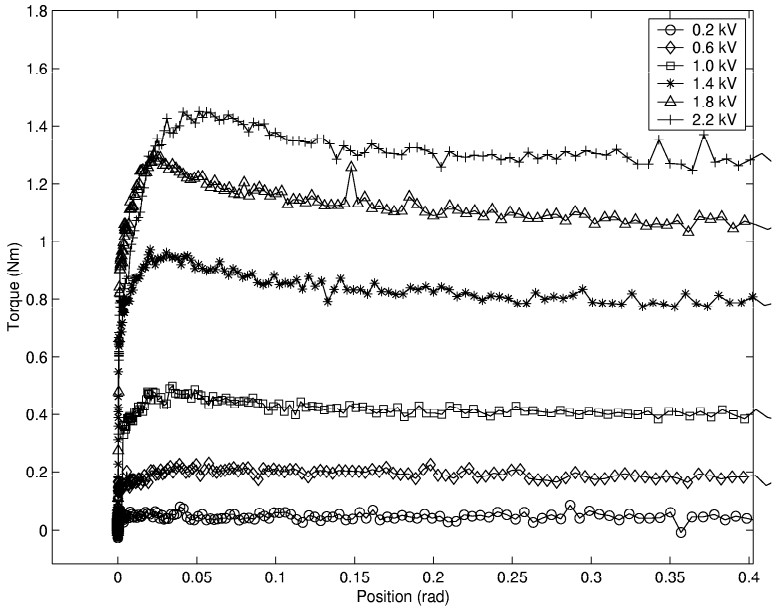

Figure 35: Relationship between torque and angular position for ER brake.

constant indicating that the fluid is now in the viscous region.

4.3 Step Response

4.3.1 Step Response to a Voltage Step Input

The step response of the device to different voltage steps was performed. For each step input, the voltage was increased from 0.2 kV to the final value, 0.5 kV, 1.0 kV, 1.5 kV and 2.0kV respectively.

Here a constant current input was given to the motor and a voltage step was applied across the electrodes of the clutch. The corresponding torque response and motor speed was measured. A Figure showing the input and measured response is shown in Figure 36. Here the lower plot shows the corresponding motor speed (solid line) and one of the voltage step inputs (dashed line) that were applied. This should give the reader an indication of the time at which step was applied.

The rise time, the time required for the response to rise from 10% to 90% of its final value, for the voltage step to 2.0 kV was measured as being 0.721 s. This response was measured without active control.

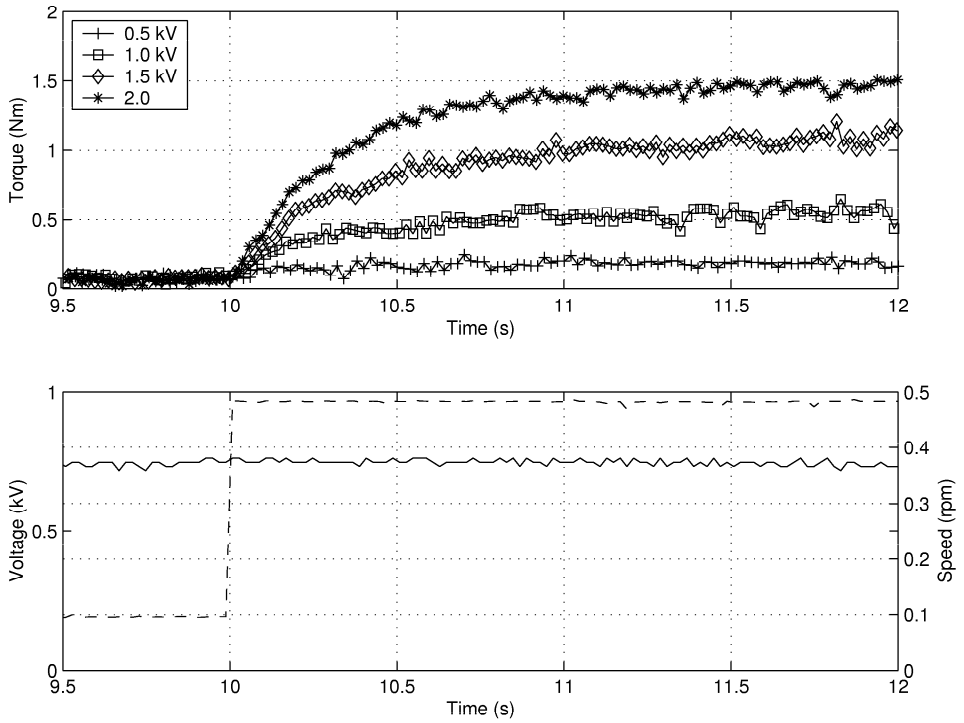

Figure 36: Step response of torque to various voltage steps at a motor velocity of 0.35 rpm

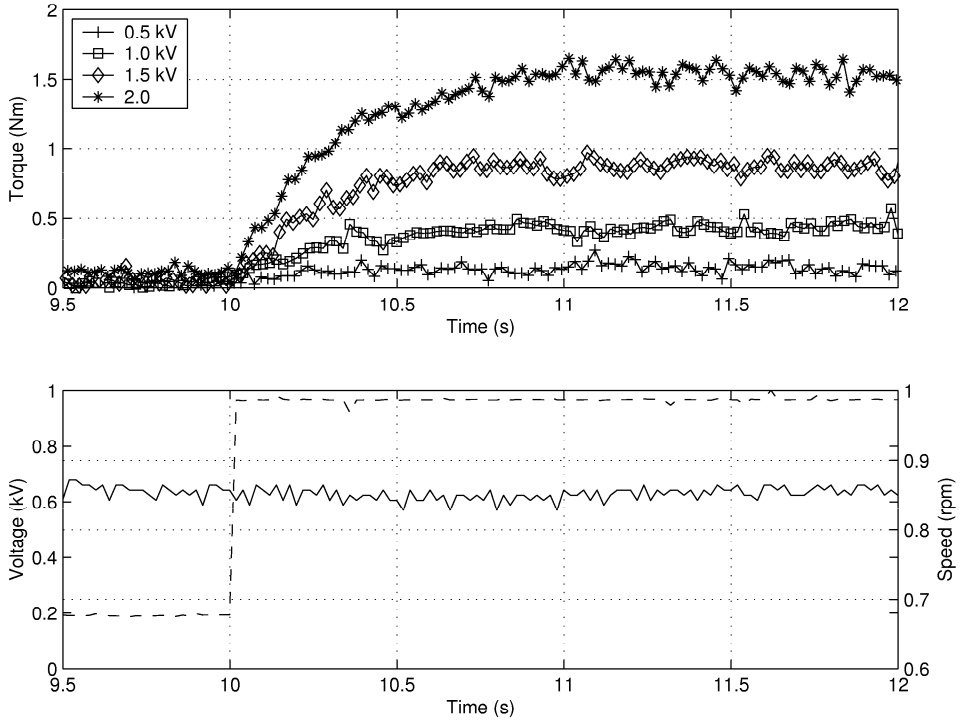

Figure 37: Step response of torque to various voltage steps at a motor velocity of 0.85 rpm

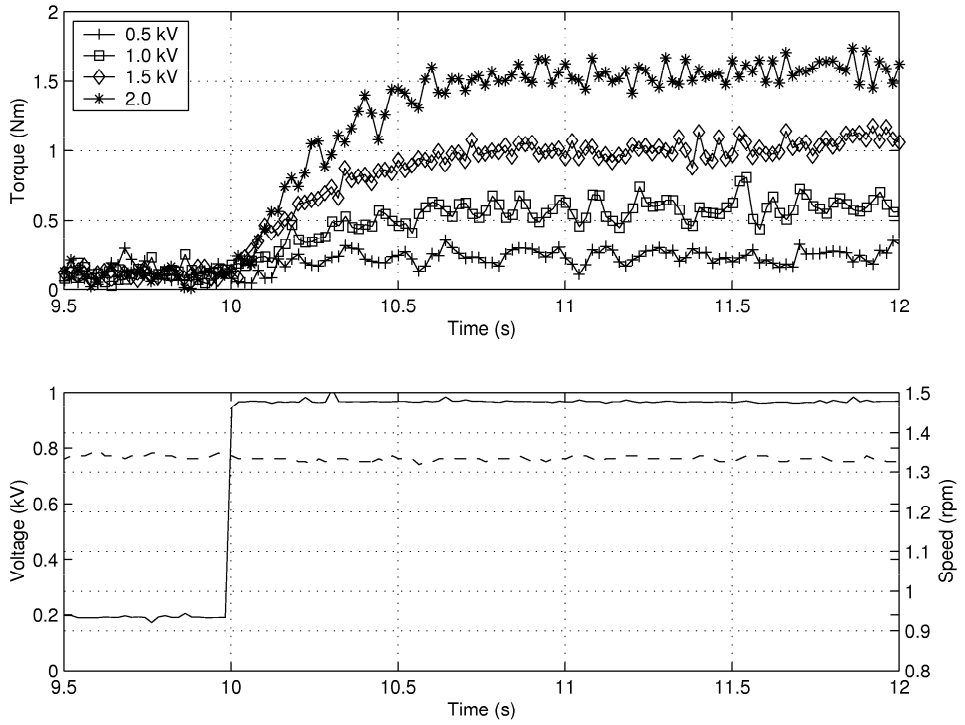

Figure 38: Step response of torque to various voltage steps at a motor velocity of 1.35 rpm

In order to determine the effect of shear rate on the response to steps in field strength, the above test was also performed for speeds of 0.85 rpm and 1.35 rpm. Results of these tests are presented in Figures 37 and 38. The rise time measured for the speed of 0.85 rpm, was calculated as being 0.580 s, while the rise time measured for a speed of 1.34 rpm was found to be 0.507 s. Table 7 shows rise times to steps of different sizes at different shear rates. With increased shear, faster rise times are possible also rise time increased with increasing step size.

This is consistent with results obtained for high speed clutches, as were presented in the literature survey.

An interesting factor to note that the rise times reported here are considerably larger than those reported in literature. (Rise times reported in literature were in the order of milliseconds). The main reason for this difference in rise times is the low shear rate used. Looking at Figure 34, the strain required to transition from the pre-yield to post yield region can be approximated as 0.05 rad.

At the highest shear rate used, 1.35 rpm, the time it takes the fluid to transition from

Table 7: Table showing rise times (from 10% to 90% of maximum) to various step inputs at different speeds.

Speed(rpm)	Voltage(kV)	Time(s)
0.35	0.5	0.315
	1.0	0.612
	1.5	0.487
	2.0	0.721
0.85	0.5	0.308
	1.0	0.418
	1.5	0.516
	2.0	0.580
1.35	0.5	0.113
	1.0	0.454
	1.5	0.461
	2.0	0.507

pre-yield to post yield is approximately 354 ms. This accounts for the slow response times measured. For a speed of 60 rpm, the corresponding transition from pre-yield to post yield would take approximately 8 ms. ER haptic devices usually function between 0 to 60rpm so the torque response time can be anywhere between 8 to 360 ms, depending on the input speed. (Note that this is without torque feedback control.)

A voltage profile was applied to the ER brake and the corresponding torque was measured. Figure 39 shows the input and the response together with the effect on motor speed shown in the lower plot. The top graph is the input to and output from the power supply, the middle plot shows the torque response, while the lower plot shows the effect of these torque changes on the motor speed.

4.3.2 Step Response to a Velocity Step Input

Since the torque equation, Equation 15, is composed of a torque dependant on velocity and a torque dependant on speed, it was decided to see what the effect, of a step input in speed, would be on the steady state output torque. This test was performed for various voltage levels, namely, 0.5 kV, 1.0 kV, 1.5 kV and 2.0 kV. Results for these tests are presented in Figure 40. The corresponding motor step input is also shown here. The results reconfirm the fact that at the shear rates under consideration, a step increase in motor speed would have negligible effect on the output torque.

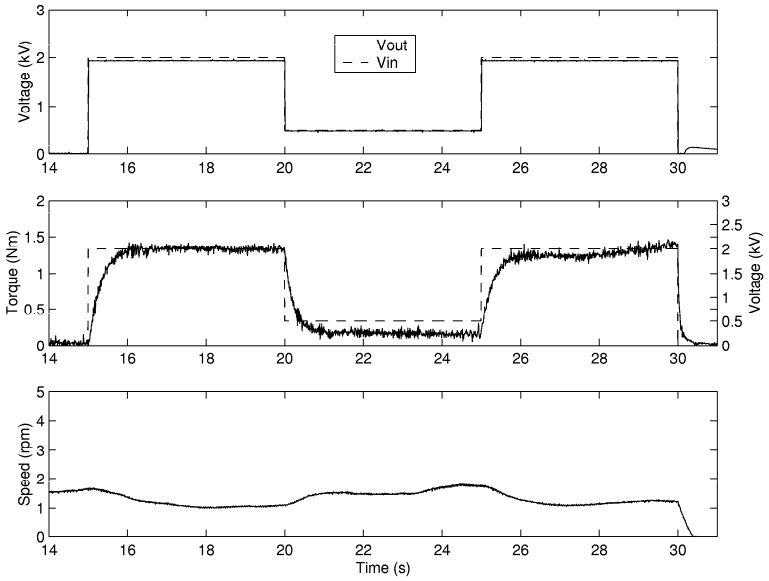

Figure 39: Figure showing torque following a specific voltage profile.

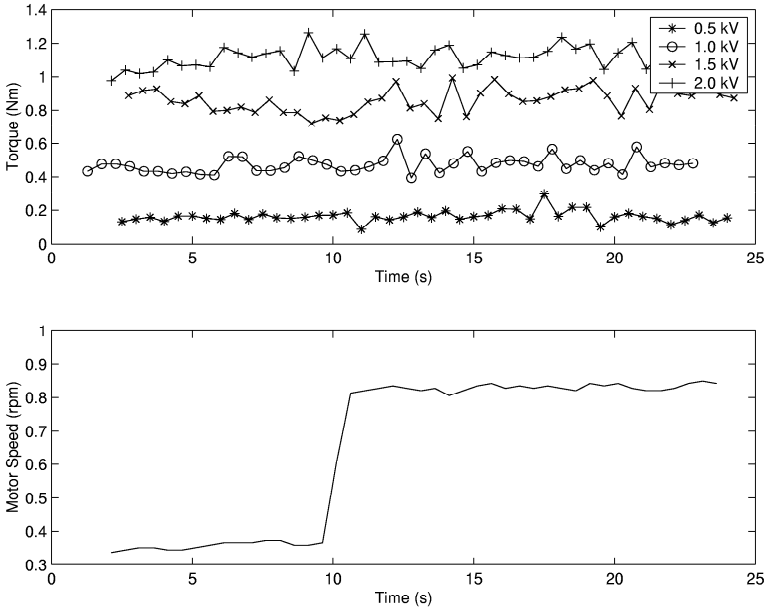

Figure 40: Figure showing step response of torque to a step input in motor speed.

4.4 Frequency Response Characteristics

4.4.1 Frequency Response Tests: Voltage Frequency Input

Frequency response tests were performed on the ER test rig to determine the frequency and phase characteristics with respect to input voltage. The frequency inputs were chirp signals (a sine wave with a frequency increasing linearly with time)with mean values of 0.5 kV, 1 kV, and 1.5 kV and amplitudes of 0.2 kV. Each test was run 10 times and the resulting phase and amplitudes were averaged. Figure 41 shows the magnitude and phase lag of the ER brake at a mean voltage of 0.5 kV.

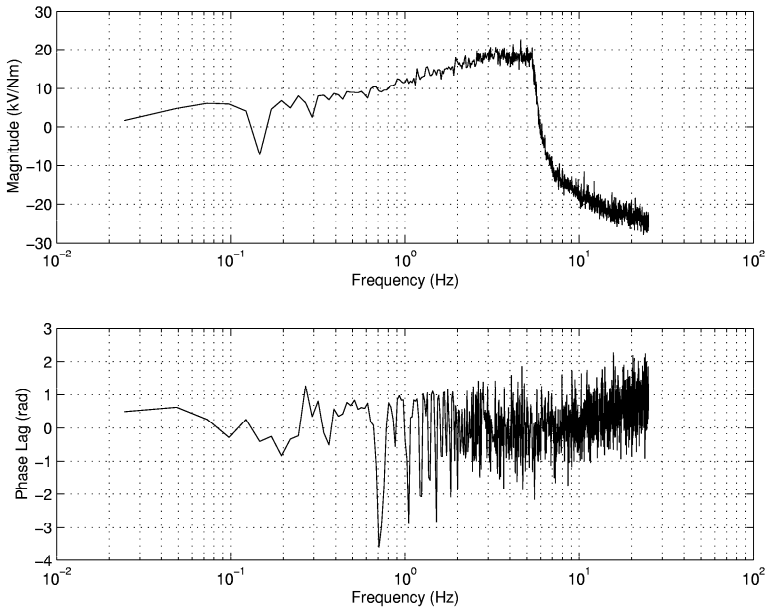

Figure 41: Figure showing the magnitude and phase lag characteristics of the ER brake at a mean voltage of 0.5 kV.

Figures 42 and 43 show frequency and phase characteristics at mean voltages of 1.0 kV and 1.5 kV respectively.

4.4.2 Frequency Response Tests: Speed Frequency Input

Frequency response tests were also performed by varying the motor speed sinusoidally at a specific voltage while measuring the torque response. This was performed for frequencies of 0.5 Hz, 1 Hz, 1.5 Hz, 2 Hz and 4 Hz.

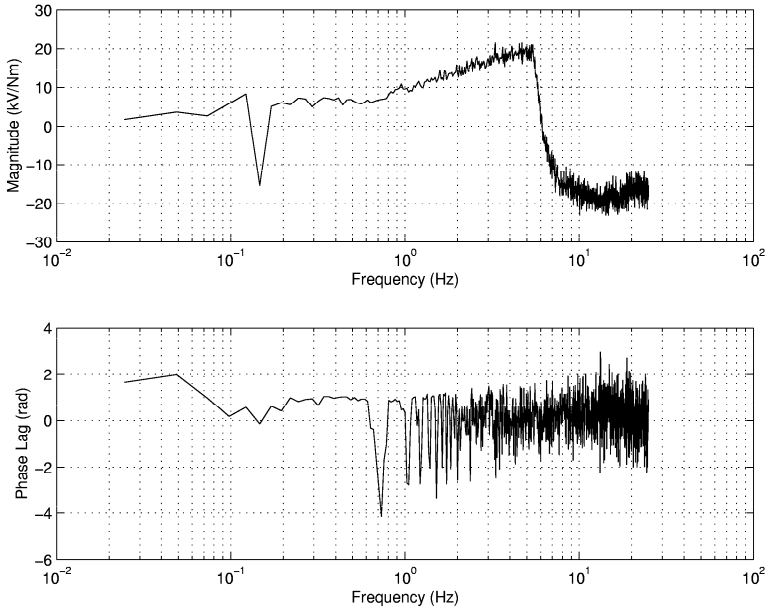

Figure 42: Figure showing the magnitude and phase lag characteristics of the ER brake at a mean voltage of 1.0 kV.

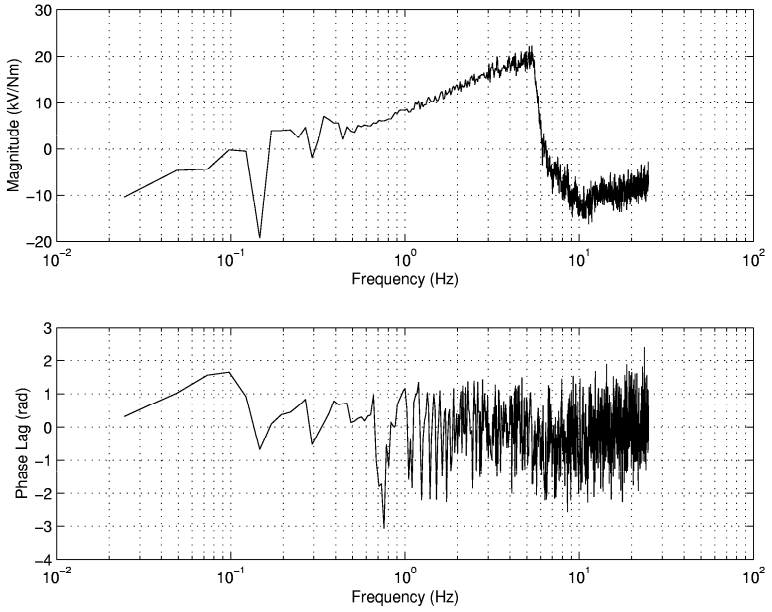

Figure 43: Figure showing the magnitude and phase lag characteristics of the ER brake at a mean voltage of 1.5 kV.

A typical data set is plotted in Figure 44. Data for this output was recorded at a frequency of 0.5 Hz and a voltage of 2.0 kV.

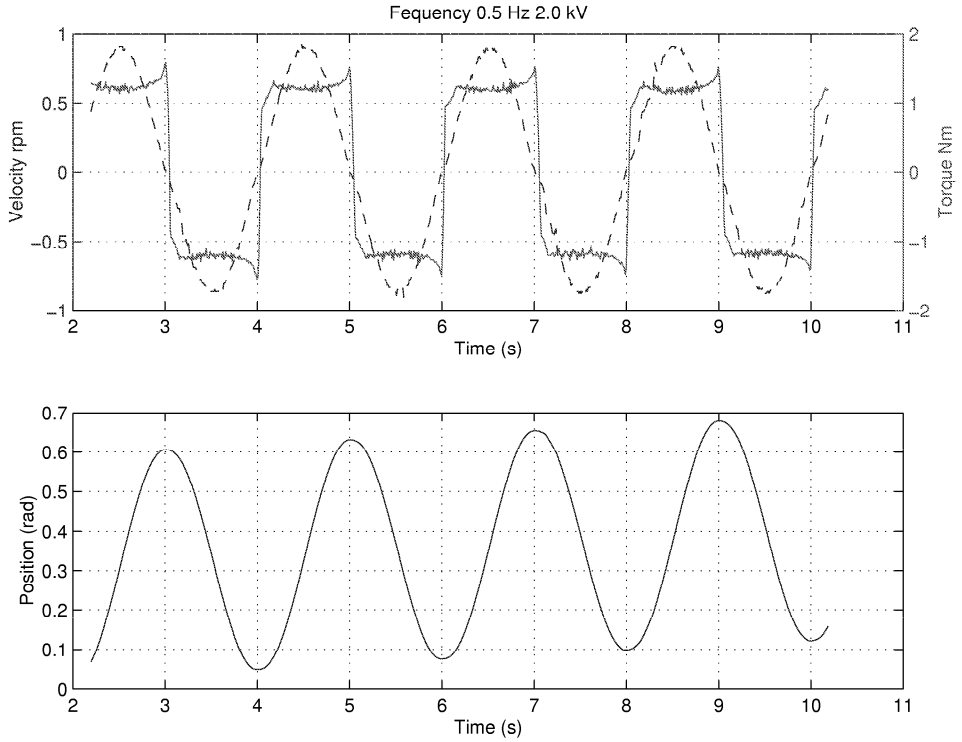

Figure 44: Figure showing the measured motor velocity, the measured rotor angular position and the measured torque response for a sinusoidal speed input of 0.5 Hz at a constant voltages of 2.0 kV.

These tests reconfirmed the above findings on speed having a negligible effect on output torque. This is reflected in the 'flat' response curves obtained. These results were consistent for all frequencies and voltages measured. There was 'no' phase change between speed input and response torque. One of the effects that the input had on the response was to reverse the direction of the torque. The negative torque has the same amplitude as its positive counterparts in each test.

Results from these tests also revealed an interesting phenomenon. As shear strain rate decreased i.e. tended towards zero, an increase in the corresponding torque response was recorded. This is clearly seen in Figure 44, at the discontinuities in the torque response plot.

To get a better understanding of this phenomenon, a shifted sinc wave input was applied

to the motor. This is shown together with the response in Figure This phenomenon can be seen occurring again where the speed gets very close to zero, by an increase in the torque response. 45.

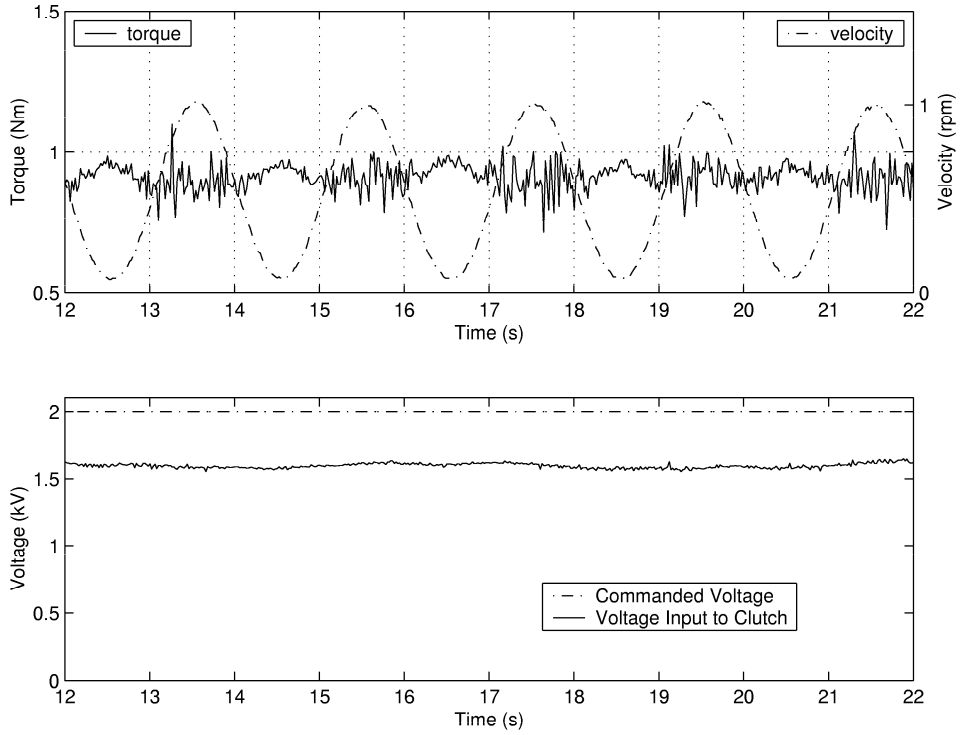

Figure 45: Figure showing the measured motor velocity, the measured torque response for a sinusoidal speed input and the resulting input and output voltages for a shifted sine input in motor speed.

In order to determine at what speeds this phenomenon occurred, a decreasing ramp was applied. Figure 46 show the speeds that were applied.

Speed was kept constant at various points along the ramp as shown in Figure 46. Results for this test are shown in the Figure 47.

This test was repeated under zero field conditions to determine whether this phenomenon was a result of the fluid properties. This phenomenon was found to be field dependent and the effect seemed to increase with increasing field.

One of the possible reasons for this observation is that ER fluids are Visco-elastic. Once they have yielded, they behave like viscous materials which respond 90 ° out of phase to a sinusoidal input. When a field is applied, this out of phase behavior becomes more

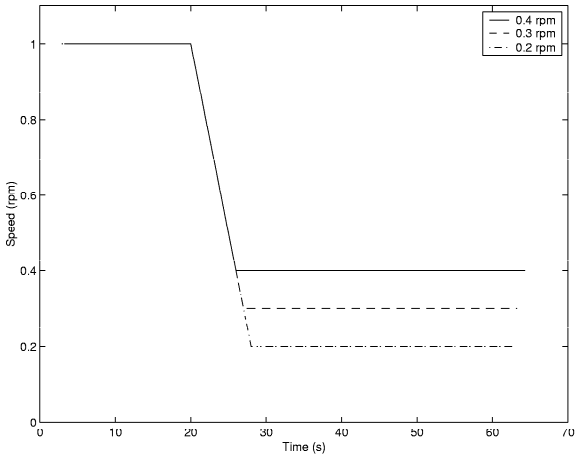

Figure 46: Figure showing the speed profile applied to the brake to determine the effect of various low speeds on the steady state torque.

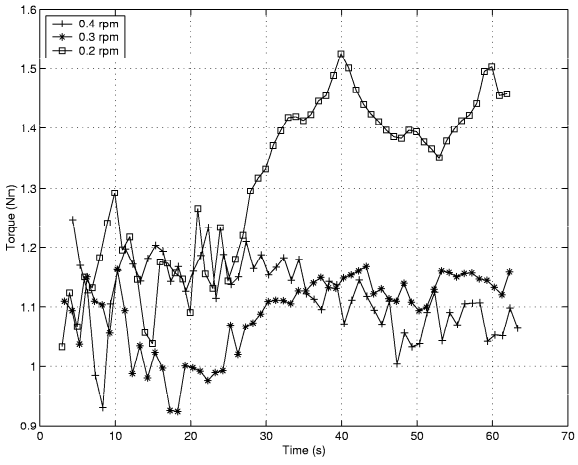

Figure 47: Figure showing the changes in output torque of the brake as speed is decreased to a small shear rate and held there.

apparent since the response curve is 'lifted' up above the mean value. Yen and Achorn [24] have reported noticing responses with higher order harmonics in the yielded region.

It was mentioned earlier that low strain rate are used for haptic purposes. The obvious question to ask now is how would this phenomenon affect the use of this device in haptic interface systems? One consequence of this phenomenon is that open loop torque control will not suffice, closed loop torque feedback control will have to be used since the steady state torque varies at low shear rates.

4.4.3 Hysteresis

Torque vs. position hysteresis data were collected. These were collected by varying the input motor speed sinusoidally and measuring the the resulting torque and position.

Figure 48 shows a hysteresis plot for torque vs. position. Figure 49 shows a hysteresis

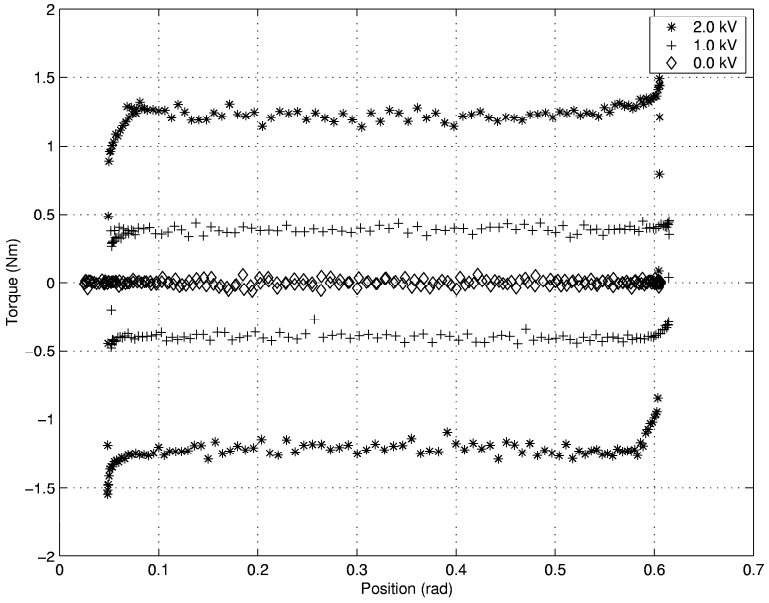

Figure 48: Hysteresis of torque vs. strain for the designed ER brake.

plot for torque vs. velocity.

These results show that hysteresis is present in the system. As voltage increases, the hysteresis effect increases as well. This is apparent in both the torque vs. velocity plots as well as the torque vs. position plots. The presence of hysteresis would have an impact on haptic systems, in that once again the need for torque feedback control becomes apparent.

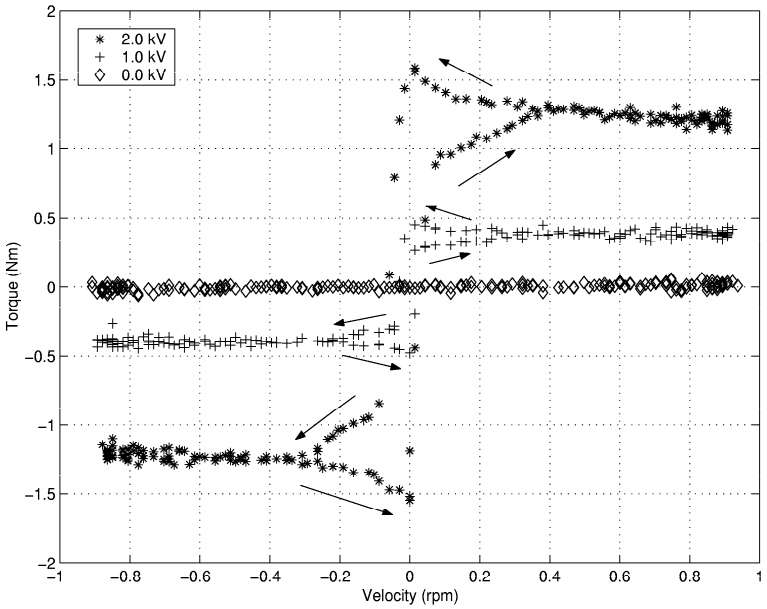

Figure 49: Hysteresis of torque vs. strain rate for the designed ER brake.

Similar findings on hysteresis were reported in dampers under high oscillation rates by Powell.

4.5 Control

4.5.1 Torque Control

Simple proportional torque feedback control was implemented. The control schematic is shown in Figure 50.

The response to a step input was measured and the results are presented below. Here the motor speed was controlled at a constant speed of 0.5 rpm. It was found that with simple feedback control rise times to steps in torque improved to approximately 43 ms (from 10% to 90% of step size). This is shown in Figure 51.

From this result it can be concluded that with simple proportional torque feedback control better response times are obtainable at the same shear rates. So, with torque feedback control in haptic systems, functioning at shear rates of between 0 to 60 rpm, much better response times in the order of milliseconds will be achievable.

Even though the response in Figure 51 is better than the response times reported earlier

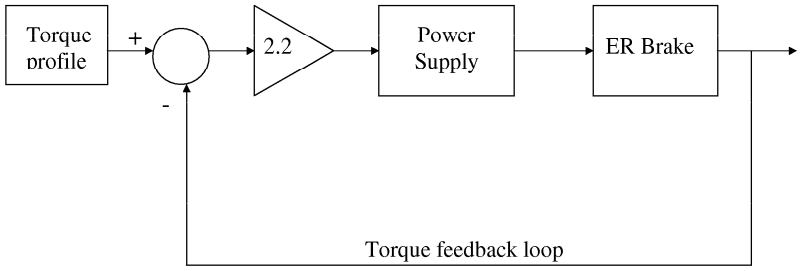

Figure 50: Figure showing a schematic of the proportional control implemented.

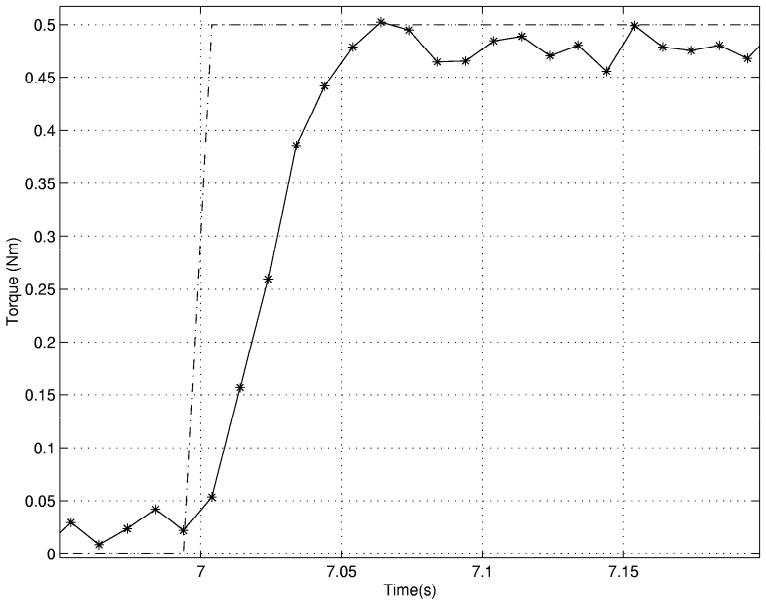

Figure 51: Step response to torque input with simple proportional feedback control.

in the text, it is still slow compared with response times reported in literature. Looking at the commanded voltage and actual voltage curves in Figure 52, it is clearly seen that a reason for this slow response is power supply saturation.

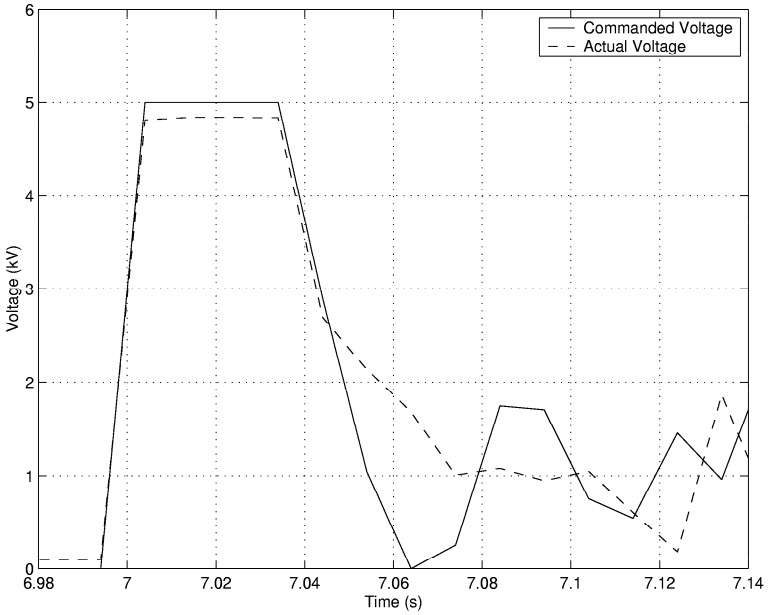

Figure 52: Figure showing the commanded and actual voltage for feedback control.

4.6 Problems Experienced

A number of problems were experienced during experimentation. These are listed below:

- The current consumption of the fluid was too high
- Arcing at voltages of about 2.5 kV were experienced.
- The maximum torque output was only 1.5 Nm, at 2.2 kV, while the clutch was designed to have an output of 5 Nm at 4 kV.
- Slow response times were experienced.
- The harmonic drive on the motor added disturbance to the system, so higher shear rates could not be investigated.

A possible reason for the high current consumption is that the outer electrode was designed to have an effective length of 100 mm, however its actual length was 115mm. This

was considered not to be a problem since actual length of the inner electrode is exactly 100 mm. However the bottom of the inner electrode is not insulated, so the possibility exists that charge is traveling from the extra 15 mm of length to the bottom of the grounded electrode. This results in a significant increase in the actual effective surface area of the brake. Hence a larger current was allowed to pass through the fluid.

Sparking in the system could be caused by the localization of charge at a notch or a 'burr' in the electrode. This could be fixed by examining the electrodes carefully for defects and re-machining or placing the electrodes where necessary.

From the above explanation it follows that lower torques are only achievable since not enough current is available to produce a larger voltage and hence increase the field strength. This coupled with the fact that the power supply was under designed accounts for lower torques being produced.

An explanation for slow response times were already given in the preceding text and will not be repeated here.

The harmonic drive and motor system used was old and should be replaced. Vibration was caused by the mating gear teeth, which ultimately affect data acquisition.

Even though the designed clutch performed poorly when compared to results for high speed clutches presented in literature, it is strongly believed that if the abovementioned problems are fixed, much better results would be obtained.

CHAPTER V

PROPOSAL FOR ER HAPTIC MANIPULATORS

Thus far in literature, only two dimensional, ER, passive haptic devices have been designed. Böse [3] proposed a spherical type manipulator, of which the design was not that successful. Furusho [20] present a linkage type manipulator which proved to be much more successful in its design i.e. it displayed good response times and had high torque to inertia ratios. Three dimensional, passive, haptic devices are yet to be designed.

Here a conceptual proposal is for a more modular concept in the design of ER haptic devices. Each brake is based on the multi-cylinder, cylindrical type design as this design makes best use of the available surface area to size of brake ratio i.e. smaller components can be built.

Figure 53 shows the basic design under consideration. This is a two degree of freedom manipulator. The design is based on the designs of existing haptic manipulators PTER (Passive Trajectory Enhancing Robots) and HURBiRT (Human Robot Bilateral Research Tool) [23].

In this design two rotating cylindrical arrangements are connected to one stationary cylindrical element. The electrodes of the rotating elements are energized by two separate high voltage power supplies. A schematic of the electrode geometries are shown in Figure 54.

This design utilizes two identical grounded electrodes attached back on back, with two identical high voltage electrodes mating with each high voltage electrode. Both the inner and outer surfaces of the cylindrical high voltage electrode contribute toward the effective surface area, this results in a reduction in length as well as the inertia of the moving electrode.

Using this concept, various other manipulator configurations can be attained. Figure 55 shows a variation of the design in Figure 53 on the left. Adding a single clutch to the

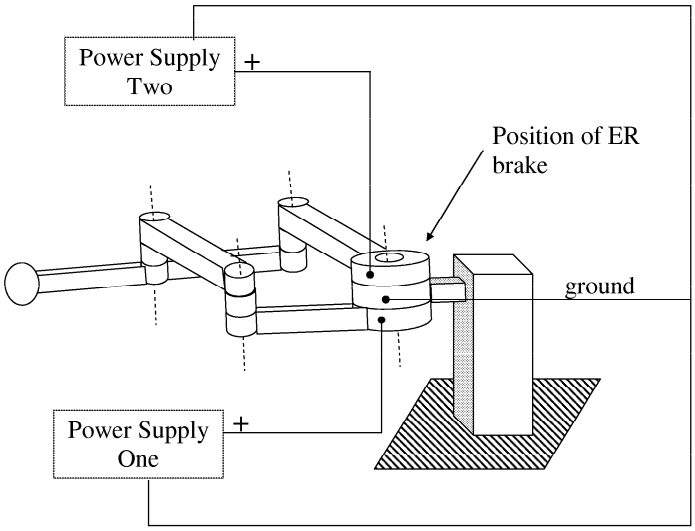

Figure 53: Figure showing a basic conceptual design for an ER, passive haptic manipulator.

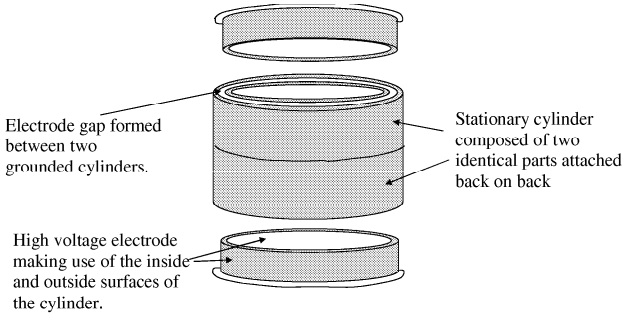

Figure 54: Figure showing details of the electrode configuration for the basic design in Figure 53.

base of this design results in a manipulator with a three dimensional workspace.

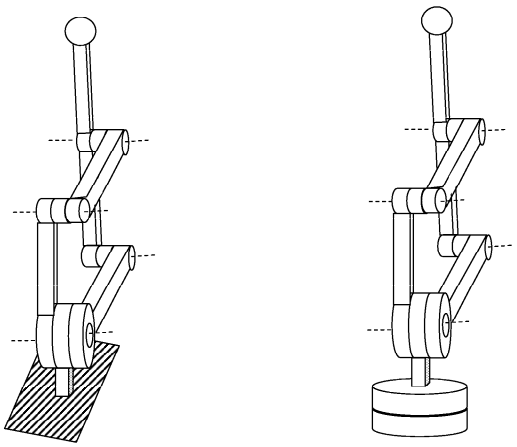

Figure 55: Figure showing an adaptation to the basic design shown in Figure 53.

The design methodology presented in Section 3.4 can be used to determine the sizes of the cylinders and hence torques that can be produced.

CHAPTER VI

CONCLUSION AND FUTURE PROPOSALS

6.1 Discussion of Results

A passive, ER brake was designed and tested with the aim of eventually using it in haptic interface system. Results obtained for these clutches were disappointing in that slow response times were observed and design torque was not attainable.

Reasons for the slow response were found to be:

- Slow shear rates
- Relatively large inertia of output member
- Power supply saturation

Shear rates between 0.3 rpm and 1.5 rpm were used in the current research. It was shown that shear rates affected the time it took for the fluid to transition from pre-yield to post-yield and if larger shear rates are used then this time is reduced to just a few milliseconds eg. at a speed of 60 rpm, the time to transition would be only 8 ms.

The inertia of the output system was calculated as being 0.0030 kg.m^2. This is considerably larger than those reported used for testing on high speed clutch systems. (Johnson et al [9] report an inertia of 4 x 10 $^{-4}$ kg.m^2.) If this inertia can be reduced, then better response times would be achievable.

In a simple proportional torque feedback control experiment conducted, it was found that the power supply saturation resulted in slow response times.

One other possible reason for slow response times was thought to be the stiffness of the harmonic drive. This was 28 225 N.m/rad and thought to be adequate since it was larger than the fluid torque constant which was caluculated as being roughly 140 N.m/rad ($K_{ER} = \frac{1.4N.m}{0.01rad}$) from Figure 35.

Reasons for not achieving design torque:

- Effective surface area larger than designed for
- Under designed power supply

After reviewing the brake design it was found that the total effective electrode area was actually larger, since the bottom of the inner electrode provided an extra grounded surface. This resulted in larger currents being drawn at lower voltages.

Further more the power supply was under designed since manufacturer catalogue data for current density required was used. Actual batch data differed from this data resulting in not enough current being produced.

The abovementioned problems are therefore attributed to design flaws and not a lack in ER fluid properties. It is still strongly believed that the response time of the fluid to change from a liquid state to a solid state is in the order of a few milliseconds. The challenge arises in designing the optimum braking device to fully enhance this characteristic.

An increase in torque was noted occurring at low strain rates. This was attributed to the viscous nature of the fluid once it had yielded. The repercussions of this finding is that open loop control of torque would not be possible in haptic systems, and feedback control would be required.

Simple proportional feedback torque control was implemented, and this was found significantly improve the rise time (time to get from 10 %-90 % of step size) to approximately 43 ms.

It is strongly believed that if the necessary design flaws are corrected and feedback torque control implemented, faster response times will be achievable.

6.2 Future Recommendations

Future proposals for the current test apparatus would be to:

- insulate the underside of the shaft and see what effect that has on sparking and current consumption.

- replace the motor to reduce the effect of vibration caused by the harmonic drive.
- decrease the electrode area so that a higher field intensity can be achieved with the current power supply.
- possibly redesign the delrin cup and outer electrode to reduce the overall inertia.
- design a three dimensional haptic ER test bed based on the proposal presented in Chapter 5.

APPENDIX A

MANUFACTURER DATA SHEETS FOR ER FLUIDS

UNDERSTANDING ER FLUIDS

A Basic Guide to the Interpretation of Data Sheets

Simple oils are specified by viscosity, density, and temperature properties. ER Fluid parameters may be less familiar; this Note is intended to explain them.

Fig. 1 shows the most basic rheological test. A flat plate, area A, is held a distance h from a flat surface with the test sample beneath it; a horizontal force, F, causes it to slide at a velocity V. The "Shear Rate" (V/h) is measured as a function of the "Shear Stress", (F/A), as shown in Fig 2. For example, in a pure liquid, or in an ER fluid without an electric field, Shear Rate is directly proportional to Shear Stress, as shown by the straight line through the origin; the slope of this line is the "Newtonian" viscosity. Other materials, including ER fluids in a field, show more complex behaviour.

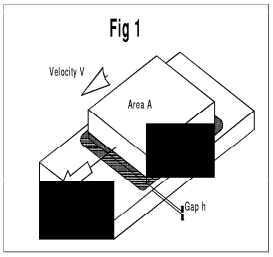

If the plates in Fig. 1 are pressed together dry, the top plate will not slid at all until the force F exceeds a limiting value, but once it is sliding, F is independent of the velocity V. In Fig. 2, this plots as a horizontal line with an intercept, Z, on the stress axis, proportional to the force pressing the plates together. In practice, "sticking" friction is usually higher than "sliding" friction, so there is a cusp on the line in Fig. 2 near the stress axis, and Z has "static" (Z^*) and dynamic (Z) values.

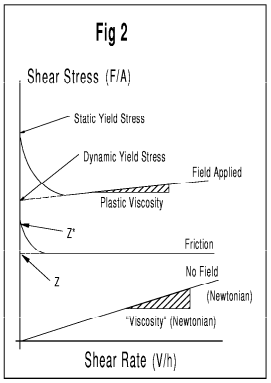

With no field, ER fluids are usually Newtonian, like normal oils. In a field, on the other hand, their behaviour resembles friction:- they will not flow at all until the Shear Stress exceeds a certain value, called the "Yield Stress", (τ). Like Z in friction, τ usually has two values, τ^* (static) being greater than τ (dynamic). However, whereas the Shear Stress/Shear Rate graph (Fig. 2) for friction is horizontal, that for ER fluids usually has a slight slope, called the "Plastic Viscosity". Static Yield Stress (τ^*), Dynamic Yield Stress, (τ) and Plastic Viscosity (μ_{pl}) are all dependent on the field (E, volts/mm) as shown in Fig. 3 - τ^* is a linear function of E above a threshold, E_o, whereas τ usually varies as E^2. μ_{pl} usually falls with E, but is sometimes constant. The coefficients in all these relationships are temperature-dependent.

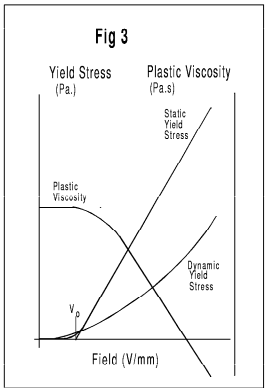

Figure 56: ER data sheets supplied by ER Fluid Developements, Ltd., Page 1.

Current

Although the current density is usually low, it is of considerable practical importance, since it determines the size (and cost) of the power supply; furthermore, high voltage units producing more than about 10mA are potentially lethal, so ER fluids and equipment must be designed to minimise current. ER fluids do not obey Ohm's law, so the current must be presented either graphically, or by reference to a model. ERFD uses a quadratic model:-

J (current density) = $PE + QE^2$

This applies to static ER fluids. This is the "worst case" since the current usually falls when flow commences. P can usually be ignored, but Q is strongly temperature-dependent. A plot of log(Q) against 1/T (°K) is linear.

No-Field Viscosity

Without a field, most ER fluids are Newtonian. No-field viscosity is an important consideration in many applications, since it determines the **minimum** torque (or pressure) that the device can produce under given conditions, just as the Yield Stress determines the maximum. The variation of no-field viscosity with temperature is usually similar to that of a pure oil.

General

The features discussed above are specific to ER Fluids. In addition, an ER Fluid must also be a "user-friendly" engineering material. The fluid should have a high boiling point and low freezing point; it should not be abrasive or attack common engineering materials; it should have a long storage and working life; it should show a minimal tendency to settle out. Above all, it must be non-toxic and safe to use.

ER fluids cannot be realistically compared on the basis of a single parameter. For example, a high yield stress at low field is obviously desirable, but if the fluid also has a high no-field viscosity, passes a high current, or cannot be used with ordinary rubber seals, it may be more trouble than it is worth in practical applications. The "best" ER fluids are those which have the best COMBINATION of desirable properties. The fluids made by ER Fluid Developments Ltd have been optimised in this way over more than 20 years.

Figure 57: ER data sheets supplied by ER Fluid Developements, Ltd., Page 2.

TECHNICAL INFORMATION SHEET

ELECTRO-RHEOLOGICAL FLUID LID 3354

PRELIMINARY
July 1998

PRODUCT DESCRIPTION

LID 3354 is an electro-rheological fluid made up of 35% by volume of polymer particles in a fluorosilicone base oil. It is designed for use as a general-purpose ER fluid with an optimal balance of critical properties and good engineering behaviour. Solid and liquid are density matched to minimise settling.

APPLICATIONS

LID 3354 can be used in suitable equipment wherever electronic control of mechanical properties is required, such as in controlled dampers, actuators, clutches, brakes and valves.

PHYSICAL PROPERTIES

Density: 1.46 x 10^3 kg/m^3
Viscosity: 125 mPa.sec at 30°C
Boiling Point: > 200°C
Flash Point: >150°C
Auto Ignition Point: N/A
Insoluble in Water
Vapour Pressure: N/A
Vapour Density: N/A
Freezing Point: < -20°C
Does not attack elastomers

STATIC YIELD STRESS AT 30°C

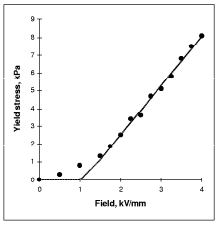

Fitted to $Y = (E-E_0).S/E$
S/E = 2.77 Pa.mm/V
E_0 = 1.09 kV/mm

DYNAMIC YIELD STRESS AT 30°C

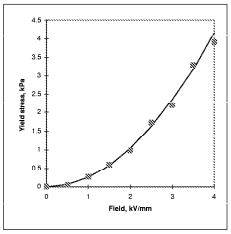

Fitted to $Y_d = A.E^2$
A = 0.26 kPa.mm^2/kV^2

PLASTIC VISCOSITY AT 30°C

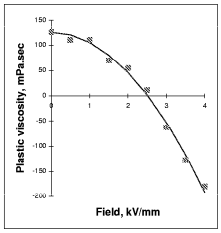

Fitted to $\mu_{pl} = \mu_0 - B.E^2$
B = 19.8 mPa.sec.mm^2/kV^2

CURRENT DENSITY AT 30°C

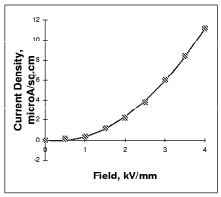

Fitted to $J = P.E + Q.E^2$
P = -4.9 x 10^{-9} A/V^2
Q = 8.2 x 10^{-15} A/V^2

Figure 58: ER data sheets supplied by ER Fluid Developements, Ltd., Page 3.

TECHNICAL INFORMATION SHEET

TEMPERATURE DEPENDENCE OF A

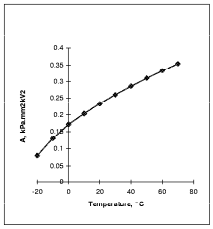

TEMPERATURE DEPENDENCE OF Q

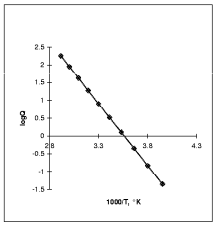

Fitted to $Q = Q_0 \exp(-\Delta H/RT)$
$\Delta H = 28.34$ kJ/mole

GENERAL INFORMATION
For safe handling of this product, consult the Material Safety Data Sheet (MSDS)

Durability
No deterioration in performance has been observed during long-term use in closed systems. Demonstration devices filled with this fluid have operated intermittently for eight years. No significant change has been seen in fluid performance.

Storage
Product can be stored in closed containers almost indefinitely at room temperature. No deterioration has been observed after storage periods of up to ten years.

Note
The data contained herein are furnished for information only and are believed to be reliable. We cannot assume responsibility for the results obtained by others over whose methods we have no control. It is the user's responsibility to determine suitability for the user's purpose of any data mentioned herein and to adopt such precautions as may be advisable for the protection of persons and of property against any hazards which may be involved in the handling and use thereof. Loctite Corporation and ER Fluid Developments Ltd specifically disclaim all warranties expressed or implied, including warranties of merchantability or fitness for a particular purpose, arising from sale or use of their products. Loctite Corporation and ER Fluid Developments Ltd specifically disclaim any liability for consequential or incidental damages of any kind, including lost profits. We recommend that each prospective user test his proposed application before repetitive use, using these data as a guide. The product is covered by one or more patents or patent applications.

For more information on ER fluids or any aspect of ER technology, contact either of the following.

Linda Evans,
ER Fluid Developments Ltd,
Vincent Works, Brough, Bradwell
Hope Valley S33 9HG, UK.
Tel: +44 1433 621449
Fax: +44 1433 620979
e-mail: erfd@compuserve.com

Kieran Mulcahy,
Loctite Corporation,
Tallaght Business Park,
Tallaght, Dublin, Ireland.
Tel: +353 1 4046570
Fax: +353 1 4510636
e-mail: kieran.mulcahy@henkel.de

Figure 59: ER data sheets supplied by ER Fluid Developements, Ltd., Page 4.

REFERENCES

[1] R. J. Atkins, Xiao Shi, and W A. Bullogh. Solution of the constitutive equations for the flow of an electrorheological fluid in radial configurations. *Journal of Rheology*, 35(7):1441–1461, October 1991.

[2] R. T. Bonnecaze and J. F. Brady. Yield stresses in electrorheological fluids. *Journal of Rheology*, 36(1):73–115, October 1991.

[3] Holger Böse and Hans-Joachim Berkemeier. Haptic device working with an electrorheological fluid. *Electro-rheological Fluids and Magneto-rheological Suspensions*, 24(5):727–734, October 1999.

[4] Douglas Brooks. Applicability of simplified expressions for design with electrorheological fluids.

[5] Torsten Butz and Oskar von Stryk. Modelling and simulation of rheological fluid devices. www-lit.ma.tum.de, May 1999.

[6] John P. Coulter, Keith D. Weiss, and J. David Carlson. Electrorheological materials and their usage in intelligent material systems and structures, part i: Mechanisms, formulations and properties. *Proceedings of the Recent Advances in Adaptive and Sensory Materials and their Applications*, pages 507–523, 1992.

[7] A. Hosseini-Sianaki, W. A. Bullough, R. Firoozian, J. Makin, and R. C. Tozer. Experimental measurements of the dynamic torque response of an electrorheological fluid in shear mode. International Journal of Modern Physics, B, June 1992.

[8] J. David Carlson John P. Coulter, Keith D. Weiss. Electrorheological materials and their usage in intelligent material systems and structures, part ii: Applications. *Proceedings of the Recent Advances in Adaptive and Sensory Materials and their Applications*, pages 507–523, 1992.

[9] A.R. Johnson, A. Hosseini-Sianaki, W. A. Bullough, R. Firoozian, J. Makin, and S. Xiao. Testing on a high speed electrorheological clutch. International Journal of Modern Physics, B, June 1992.

[10] Therese C. Jordan and Mongomerey T. Shaw. Electro-rheology. *IEEE Transactions on Electrical InsulationJournal*, 24(5):849–878, October 1989.

[11] Gopalakrishna M. Kamath and Norman M. Wereley. A nonlinear visoelastic-plastic model for electrorheological fluids. IOP Publishing Limited, February 1997.

[12] K. S. Kim, S. B. Choi, and M. S. Cho. Vibration control of a wire cut discharge machine using er brake actuator. World Scientific, March 2000.

[13] D. Lampe. Materials database on commercially available er and mr fluids. http://www.tu-dresden.de/mwilr/lampe/HAUENG.HTM, January 1997.

[14] C. Mavroidis, C. Pfeiffer, J. Celestino, and Y. Bar-Cohen. Controlled compliance haptic interface using electro-rheological fluids. Proceedings of the SPIE Conference on EAPAD, March 2000.

[15] S. Munir, L. Tognetti, and W. J. Book. Experimental evaluation of a new breaking system for use in passive haptic displays. Proceddings of the American Control Conference, June 1999.

[16] Masamichi Sakaguchi and Junji Furusho. New actuators utilizing er fluids anf their applications to force display devices in virtual reality and medical treatments. *Electro-rheological Fluids, Magneto-rheological Suspensions and their Applications*, 24(5):755–763, July 1997.

[17] Masamichi Sakaguchi and Junji Furusho. Force display system using particle-type electrorheological fluids. *IEEE International Conference on Robotics and Automation*, 24(5):2586–2591, May 1998.

[18] Masamichi Sakaguchi and Junji Furusho. Developement of 2 dof force display system using er actuators. *IEEE?ASME International Conference on Advanced Intelligent Mechatronics*, 24(5):707–712, September 1999.

[19] Masamichi Sakaguchi, Junji Furusho, and Eiichi Genda. Basic study on rehabilitation training systems using er actuators. *IEEE*, 24(5):135–140, July 1999.

[20] Masamichi Sakaguchi, Junji Furusho, and Naoyuki Takasue. Passive force display using er brakes and its control experiments. *IEEE*, 24(5):7–12, July 2001.

[21] Masamichi Sakaguchi, Junji Furusho, and Guoguang Zhang. Modelling and motion control of an actuator unit using er clutches. *IEEE International Conference on Robotics and Automation*, 24(5):1347–1353, April 2000.

[22] A. V. Srinivasan and Michael McFarland. *Smart Structures: Analysis and Design.* Cambridge University Press, 1 edition, 2001.

[23] Lawrence Joseph Tognetti. *Actuator Design for Passive Haptic Display.* Masters dissertation, Georgia Institute of Technology, Department of Mechnical Engineering, June 1999.

[24] W.S. Yen and P.J. Achorn. A study of the dynamic behaviour of an electrorheological fluid. *J. of Rheology*, 35(7):1375–1384, March 1991.